Cyclotron Production of ^{68}Ga using a ^{68}Zn-based liquid target

Hugo Manuel Ramos Moreira

To my parents,

Cyclotron Production of ^{68}Ga using a ^{68}Zn-based liquid target

Hugo Manuel Ramos Moreira

Supervisor: Francisco José Cerqueira Alves
Co-supervisor: Antero José Pena Afonso de Abrunhosa

Dissertation presented to the Faculty of Sciences
and Technology of the University of Coimbra to
obtain a Master's degree in Biomedical Engineering

Physics Department
Faculty of Sciences and Technology of University of Coimbra
2013

Acknowledgments

To my supervisor Francisco Alves, for all his support, motivation, advice and confidence in me. The most smiling science experienced person I ever met.

To professor Antero Abrunhosa, for his help and guidance through all my work. I am grateful for the indescribable opportunity he gave me.

To professor Artur Valente, from the Chemistry Department, for all the moments of discussion, supervision and assistance during the year. Without him I would never accomplish this work goals.

To all the ICNAS team, especially Vítor Alves, Sérgio Carmo and Nuno Ferreira, for all the brainstorms, suggestions and help provided during the project. Their interest and contribution were indispensable.

To professor Miguel Morgado, coordinator of the Biomedical Engineering course, for his work, assistance and important advices for the students.

To all my friends and colleagues in Coimbra, especially Daniel, Gonçalo, Elizabete, Cláudia, Pedro, João, António, Laura, Diana and Samuel, for their support, smiles and motivation during these 5 years, but mostly for their unquestionable friendship.

To my hometown friends, Miguel, Gonçalo, Leandro, Ana, Helena, Ricardo, João and Pedro, they helped me become who I am during the many years I grew up with them. Our friendship becomes more strengthened each year.

To Ana Luísa, for all the moments of affection, encouragement and motivation to never give up.

To my goddaughter wedding Sofia and her husband Pedro, for their trust, laughs, and pride in me. More than friends, they are family.

To my family, especially my grandparents Emília and Armando, my uncles Manuel and Nadir, as well as my cousins Ana, Áurea, Nando and Zé. I owe them too much.

Finally, and more importantly, to my parents Áurea and Manuel. Without their love, support, wisdom and trust in me, I would never reach this goal. Thank you for everything.

ii

Abstract

Recent research developments have demonstrated significant advantages of Gallium-68 labeled radiopharmaceuticals in PET cancer imaging, namely on neuroendocrine tumours. The suitable half-life (68 minutes), high positron emission yield and low radiation exposure for the patient are some of the main advantages that increasingly awake the interest in the use of ^{68}Ga. The research for simpler and efficient methods of ^{68}Ga production with high yields is constant.

In this work, the feasibility of a new pathway for ^{68}Ga cyclotron production, based on a liquid target through a ^{68}Zn(p,n)^{68}Ga nuclear reaction, was studied.

A salt solution of natural zinc chloride is chosen as liquid target, having suitable chemical properties for cyclotron irradiation. The 18.75 % abundance of ^{68}Zn in ^{nat}Zn is suitable for cost effective high ^{68}Ga production yields.

Niobium, widely used in cyclotron applications, is considered as target chamber material to hold the target solution. The physicochemical effect of zinc chloride solutions in the metal is studied and analyzed, in order to ensure its resistance to the irradiation conditions. This analysis is performed with scanning electron microscopy and energy dispersive X-ray spectroscopy, after exposing niobium samples to $ZnCl_2$ solutions. The effect of zinc chloride is also studied in teflon, intended to be used to transport the target solution from the cyclotron to hot-cells. For that purpose, a thermogravimetric analysis is done.

Irradiation tests are performed, with identification of the produced gallium isotopes, as well as their production yields. Different separation methods for gallium extraction are studied, by using ion exchange columns. The method with the best results is applied to a final ^{68}Ga production, having obtained excellent gallium column absorption levels.

Keywords: PET, Gallium-68, neuroendocrine tumours, cyclotron, liquid target, ion exchange columns.

Resumo

Desenvolvimentos recentes no estudo científico têm demonstrado vantagens significativas de radiofármacos marcados com Gálio-68 em imagem PET de cancros, nomeadamente para tumores neuroendócrinos. O conveniente período de semi-desintegração (68 minutos), a alta probabilidade de emissão de positrões e a baixa exposição à radiação para o doente são algumas das principais vantagens que têm vindo a despertar cada vez mais o interesse para o uso de ^{68}Ga. A procura por métodos mais simples e eficientes para a produção de ^{68}Ga com elevados rendimentos é constante.

Neste trabalho foi estudada a viabilidade de um novo método de produção em ciclotrão de ^{68}Ga, baseado num alvo líquido através da reação nuclear ^{68}Zn(p,n)^{68}Ga.

Uma solução salina de cloreto de zinco natural é escolhida como alvo líquido, tendo propriedades químicas adequadas para uma irradiação em ciclotrão. A presença de 18.75 % de ^{68}Zn em ^{nat}Zn é apropriada para rendimentos de produção elevados de ^{68}Ga.

O nióbio, bastante usado em aplicações em ciclotrão, é considerado como material para suporte do alvo, de forma a conter a solução-alvo. O efeito fisicoquímico de soluções de cloreto de zinco no metal é estudado e analisado, de forma a assegurar a resistência às condições de irradiação. A análise é feita através de microscopia eletrónica de varrimento e espetroscopia de raios-X por energia dispersiva, após exposição de amostras de nióbio a soluções de ZnCl$_2$. O efeito de cloreto de zinco é também estudado em teflon, pretendido para ser usado no transporte da solução-alvo do ciclotrão para células quentes. Com esse intuito, é feita uma análise termogravimétrica.

Testes de irradiação são realizados, com a identificação dos isótopos de gálio produzidos, assim como os seus rendimentos de produção. Diferentes métodos de separação para extração de gálio são estudados, através do uso de colunas de troca iónica. O método com os melhores resultados é aplicado a uma produção final de ^{68}Ga, tendo-se obtido excelentes níveis de absorção de gálio na coluna.

Palavras chave: PET, Gálio-68, tumores neuroendócrinos, ciclotrão, alvo líquido, colunas de troca iónica.

Index

List of Figures

List of Tables

x

Acronyms

B	Magnetic Field induction
BGO	Bismuth Germanate
cpm	counts per minute
CT	Computed Tomography
d	deuterium
DOTA	1,4,7,10-tetraazacyclododecane-1,4,7,10-tetraacetic acid
DTG	First derivative curve of the TGA
DTPA	Diethylenetriaminepentaaceticacid
e.g	*exempli gratia* ("for example")
EC	Electron Capture
EDS	Energy Dispersive X-ray Spectroscopy
EOB	End of Bombardment
f	Frequency
FDG	2-[^{18}F]-fluoro-2-deoxy-D-glucose
F_f	Centrifugal Force
F_L	Lorentz Force
F_p	Centripetal Force
FWHM	Full width at half maximum
GEP-NETs	Gastroenteropancreatic neuroendocrine tumours
GSO	Cerium-doped Gadolinium Oxyorthosilicate
HRCT	High Resolution Computed Tomography
ICNAS	Instituto de Ciências Nucleares Aplicadas à Saúde
ICR	Ion Cylotron Resonance
IPN	Instituto Pedro Nunes
LSO	Cerium-doped Lutetium Oxyorthosilicate
M	Molar
m	Mass
MRI	Magnetic Resonance Imaging

n	Neutron
NET	Neuroendocrine Tumour
NaI(Tl)	Thallium-doped Sodium Iodide
p	Proton
PET	Positron Emission Tomography
Q	Charge of the particle
r	Radius of Orbit
SEER	Surveillance Epidemiology and End Results database
SEM	Scanning Electron Microscopy
SPECT	Single Photon Emission Computed Tomography
SST	Somatostatin
SSTR	Somatostatin Receptor
T	Kinetic Energy
$t_{1/2}$	Half-life
TGA	Thermogravimetric Analysis
U	Potential difference
US	United States of America
v	Velocity
WHO	World Health Organization
wt	weight percent
Z_{eff}	Effective atomic number
β^+	Positron
β^-	Electron
γ	Gamma photon
ω	Angular velocity of the accelerated particle
ω_E	Angular velocity of the alternating current source
μ	Linear attenuation coefficient
τ	**PET** coincidence timing window

Isotopes and Chemical Elements

^{37}Ar	Argon-37
^{11}C	Carbon-11
^{37}Cl	Chloride-37
^{18}F	Fluorine-18
^{66}Ga	Gallium-66
^{67}Ga	Gallium-67
^{68}Ga	Gallium-68
^{68}Ge	Germanium-68
^{111}In	Indium-111
^{13}N	Nitrogen-13
^{14}N	Nitrogen-14
^{15}O	Oxygen-15
^{16}O	Oxygen-16
^{18}O	Oxygen-18
^{82}Rb	Rubidium-82
^{82}Sr	Strontium-82
^{99m}Tc	Metastable form of Technetium-99
^{64}Zn	Zinc-64
^{66}Zn	Zinc-66
^{67}Zn	Zinc-67
^{68}Zn	Zinc-68
^{70}Zn	Zinc-70
^{nat}Zn	Natural form of Zinc
Nb	Niobium

1. Introduction

Part I: Final Project

The final year project in M.Sc. Biomedical Engineering is done during one year, having started on September 2012.

During the first academic semester, a familiarization with the theoretical background on the significant topics related to the proposed project was conducted. It was additionally made a literature research for the possible methods, techniques and suitable materials to be used in the fulfillment of the intended objectives.

In the second semester, the implementation of the necessary and studied analysis techniques was performed. The M.Sc. thesis was also written during that time, as the results were obtained.

1.1. Objectives

The aim of this work is to evaluate and test the hypothesis of producing ^{68}Ga with a Zn based liquid target solution, by a cyclotron proton irradiation. For that purpose, it is necessary to accomplish the given objectives:

- Access and study zinc based solutions with suitable physicochemical properties for cyclotron production
- Select the target chamber and window material, testing the chemical effect of the target solution on it
- Ensure the resistance of the transfer line tubes, used to transport the final product

- Research and test methods to separate and extract ^{68}Ga from the chosen zinc solution

- Produce ^{68}Ga through cyclotron proton bombardment of the target solution, identifying its presence and production yields

- Separate and retain the produced gallium isotopes

Figure 1.1 shows the schematic plan of the objectives and steps during the project timeline.
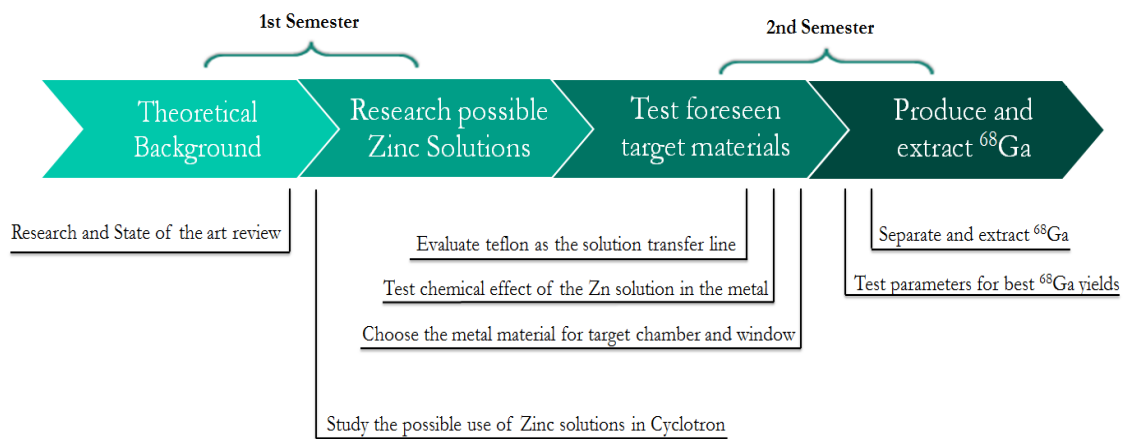
Figure 1.1 Schematic diagram of the steps involved in the production of ^{68}Ga using a Zn-based liquid target.

The final M.Sc. project was done in ICNAS (Instituto de Ciências Nucleares Aplicadas à Saúde), with the collaboration of the Chemistry Department of the University of Coimbra.

Part II: Theoretical Introduction

1.2. Neuroendocrine Tumours

Well differentiated neoplasms of the disseminated neuroendocrine cells are classified by the WHO (World Health Organization) as neuroendocrine tumours (NETs). In the last three decades there have been considerable advances in the research of these tumours, more specifically in the most common gastroenteropancreatic neuroendocrine tumours (GEP-NETs). Our understanding of the underlying pathophysiology has considerably increased, allowing for better diagnosis and more effective treatments for the patients [1, 2].

Even if some diagnosed NETs appear to have a benign behavior, all of them are potentially malignant, which makes this specific type of tumours particularly dangerous [3]. Although all NETs share an endocrine origin, their location in the body can considerably vary, appearing in organs such as stomach, duodenum, pancreas, small intestine, appendix, colon or rectum [4-7].

Neuroendocrine tumours are known to overexpress somatostatin (SST) receptors in most of their cells [8]. SST is a neuropeptide, mainly secreted in the stomach and intestine, capable of inhibiting the release and the action of all known gastrointestinal tract hormones [9].

1.2.1. Epidemology

In the past few decades, developments in image diagnosis techniques have rapidly expanded. This also translated the evidence of an increasing detection of neuroendocrine tumours, particularly GEP-NETs. According to data from the database of the Surveillance Epidemiology and End Results database (SEER) of the US National Center Institute, GEP-NETs have shown a surprising increase in 30 years, for instance of 460 % in the small intestine and 720% in the digestive system [10]. An extensive analysis of the incidence in the past decades of carcinoid tumours, related to NETs, can be found in Figure 1.2.
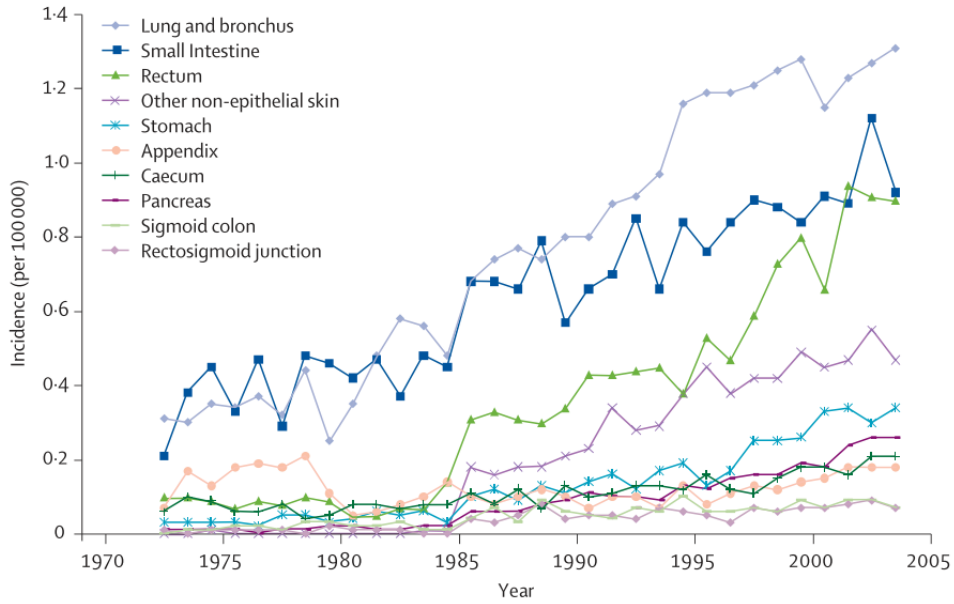
Figure 1.2 Analysis of the incidence of carcinoid tumours in the US population in the last decades [10].

The need of improvement, expansion and research of radiological imaging techniques that allow an earlier and better diagnosis was, and still is, essential as a prevention response to the NETs consequences.

1.3. In vivo Imaging

Neuroendocrine tumours can be diagnosed by conventional imaging techniques, such as computed tomography (CT) and magnetic resonance imaging (MRI) or evaluated using nuclear medicine approaches.

1.3.1. CT and MRI in NETs Imaging

CT and MRI have been widely used to detect different tumours, also having an important role in the case of NETs [11]. A short description of the techniques and their use in NETs diagnosis is described.

1.3.1.1. Computed Tomography (CT)

CT produces digital and anatomic cross-sectional images of a patient by the reconstruction of the transmitted x-rays detected in the system. The main principle is based on the transmission of an x-ray beam, with a given intensity I_0, through the targeted patient area. This beam is attenuated when passing through matter, with different attenuation coefficients μ for different mediums. The transmitted beam, with an intensity I, is detected and processed, being later analyzed though the reconstructed image. Image reconstruction is done based on the x-ray attenuation principle. Accordingly to the tissue thickness and attenuation coefficient, the transmitted beam intensity I can be related to the described parameters by the Lambert-Beer's law [12]:

$$I = I_0 e^{-\mu x}$$
<div align="right">Eq. 1.1</div>

CT sensitivity for NETs varies with the tumour location and size. In the case of pancreatic NETs, when using non-spiral CT, tumours with smaller sizes than 1 cm have not been detected. Sensitivity for tumours with sizes between 1 and 3 cm can go up to 30%, reaching to higher values of 95% for sizes superior to 3 cm. The full sensitivity range for these tumours, reported between 29 to 78%, is consequently not very reliable [11]. In NET studies using high resolution computed tomography (HRCT), the results were also not satisfactory [13].

1.3.1.2. Magnetic Resonance Imaging (MRI)

Magnetic resonance imaging is a multidisciplinary image modality that does not use ionizing radiation to detect NETs [11, 14]

This technique is based on the interaction of a strong applied magnetic field to a patient with its tissue protons. A human tissue can be composed by 70 to 90 % of water, rich in hydrogen nuclei and consequently protons. These protons have different spins. A magnetic field excites the hydrogen nuclei. When submitted to a magnetic field, protons line up in the direction of the field. Radio frequency signals are emitted, inducing transitions between spin states. When the radio frequency signal is turned off, a relaxation of the spins occurs, back to their original state. During this relaxation, protons emit low radio frequency signals that can be detected and later used to form tissue cross-section images.

This interaction allows the MRI to be very sensitive to the water densities changes between tissues, consequently related to diseases and injuries. The amount of water in an injured tissue can be significantly altered. Hence, this image modality can study the tissue function [14].

In the case of NETs, MRI detection sensitivities are comparable and most of the times similar to the ones reported with CT. Although magnetic resonance imaging can detect slightly smaller tumours than the ones reported with computed tomography, it still presents many difficulties and poor results [11, 15].

Despite the results for detecting NETs by using CT or MRI systems, it is essential to identify and diagnose such tumour pathologies in the earlier stages, when the tumours still present small sizes. Diagnosis and consequent treatment risks are highly dependent on the tumour stage. These techniques can be combined instead with stronger NET image modalities, such as PET, as a support [11, 16].

1.3.2.   Positron Emission Tomography

Positron Emission Tomography (PET) is a non-invasive nuclear technique that allows us to map, *in vivo*, molecular pathways and interactions in order to detect and analyze a variety of pathologies [17, 18].

In PET, positron emission radioisotopes are used to label compounds as molecular probes or radiotracers for biological and biochemical analysis *in vivo*. These labeled molecules, called radiopharmaceuticals, are injected, most of the times intravenously. PET image scans will provide the information of the concentration and location of the radiopharmaceutical in the organism, during the time the exam is being performed [19].

1.3.2.1. Positron Emission Tomography Principles

The principle of PET starts with a positron (β^+ particle) release by the nuclei of a specific radiopharmaceutical. When ejected, the positron loses energy in the travelled distance by interacting with matter, up to the point it collides with its antiparticle, an electron (β^- particle) [20]. This positron-electron pair collision leads to an annihilation

process. Consequently, the annihilated pair is physically converted into two collinear gamma rays with energies of 511 keV, travelling in opposite directions, as Figure 1.3 (A) illustrates. These two gamma rays can be detected in a PET detector ring, like demonstrated in Figure 1.3 (B) [21, 22].
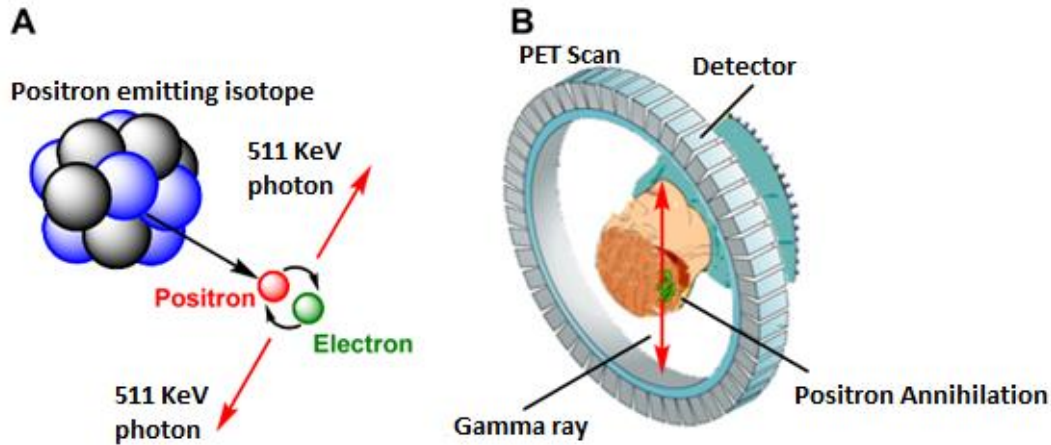
Figure 1.3 - Release of a positron, followed by its annihilation with an electron. It results in two 511 keV gamma rays traveling in opposite directions (A). Coincidence event detected by the PET ring of detectors (B). Adapted from [22].

One of the biggest advantages of PET is related to the known energy window of the two detected gamma rays. Because of the conserve energy and momentum principles, the total energy of the two annihilation gamma rays must correspond to the sum of the rest mass energies of the two collided β particles, i.e. 1.22 MeV. This annihilation coincidence detection allows the system not to require an absorptive collimator, resulting in a better sensitivity for PET, when compared with other techniques. Each detected single photon is counted and a true coincidence event is identified when the annihilation pair of photons is counted by coincidence detectors within a timing window τ. This coincidence timing window defines the maximum time interval where two 511 keV photons are counted as a true event. The τ value can usually vary around 6 to 12 ns [21, 23].

Multiple counts of true events in the system, together with the applied reconstruction algorithms, allow the output and reconstruction of a 3D image that maps the different concentrations and distribution of the radiopharmaceutical in the organism [23].

There are still some limitations in PET, regarding its spatial resolution. First, the annihilation event does not occur at the same time and location as the positron release. Before annihilated, the positron first travels a finite distance from the decaying nucleus. It

interacts with other nuclei and particles present in the matter until it collides with an electron. Only then can the annihilation event occur. Secondly, the two resulting gamma photons are not exactly collinear. In the moment of annihilation, the positron still has residual momentum and kinetic energy. Due to the conserve of momentum principle, the two photons are emitted 180 ± 0.25^{0} apart from each other. Figure 1.4 demonstrates the described physical aspects of PET positron annihilation and their effects on spatial resolution. Despite these limitations, there are spatial correction algorithms that can be applied in the image reconstruction process [21].
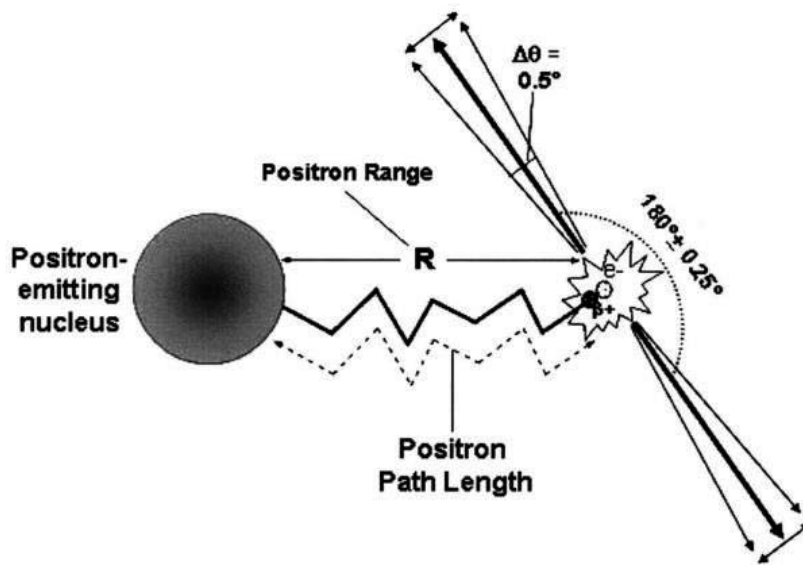
Figure 1.4 Representation of PET physical limitations in spatial resolution. Adapted from [21]

1.3.2.2. Crystal Detectors Types

Detector materials in PET are one of the most important factors that allow a correct output signal and diagnosis obtained. In order to do that, the detector material, based on scintillation, needs to have a good detection probability as well as an excellent energy resolution.

The most important properties of a scintillation detector material to obtain the best signal outputs are its mass density (ρ), effective atomic number (Z_{eff}), light output and scintillation decay time. A high mass density and effective atomic number allow a higher crystal stopping power and linear attenuation coefficient (μ). These properties are responsible for a better probability of radiation interaction and detection. A high light

output reduces the statistical noise in the scintillation, allowing better energy resolutions. A crystal with a fast scintillation decay time gives the chance of using a narrow coincidence timing window, which leads to a reduction of random count rates [21].

Most common inorganic scintillator crystals used for PET detectors are made of bismuth germanate (BGO), cerium-doped lutetium oxyorthosilicate (LSO) or cerium-doped gadolinium oxyorthosilicate (GSO). Table 1.1 shows some of their main properties comparing with the ones of thallium-doped sodium iodide (NaI(Tl)), a historic standard crystal for photon detection.

Table 1.1 Physical properties of the most common PET Scintillator materials. Adapted from [21]

	BGO	GSO	LSO	NaI(TI)
Density ϱ (g/cm^3)	7,1	6,7	7,4	3,7
Effective Atomic Number Z_{eff}	75	59	66	51
Linear Attenuation Coefficient μ, for 511 keV photons (cm^{-1})	0,95	0.70	0.88	0.34
Relative Probability of Photoelectric Interaction (%)	40	25	32	17
Light Output (photons per MeV)	9000	8000	30000	41000
Scintillation Decay Time (ns)	300	60	40	230
Energy Resolution at 511 keV (% FWHM[1])	12	9	10	8

As Table 1.1 shows, LSO crystal materials have emerged as one of the best PET detectors. Its high attenuation coefficient and light output, together with its fast scintillation decay and low energy resolution make it an excellent PET crystal detector.

---

[1] Full width at half maximum

1.3.3. Radiopharmaceuticals

A radiopharmaceutical is a radiolabelled molecule produced for *in vivo* applications. It is composed of two main parts. The first is a biomolecule structure responsible for the binding location of the radiopharmaceutical in the organism, since its structure determines the pathways and interactions of the molecule in the living organism. In the case of neuroendocrine tumours, the ligand is usually an SST analogue. The second part is a radioactive nuclide responsible for the signal detection [24, 25].

1.3.3.1. Radiopharmaceuticals in PET

In the case of PET, the radioactive nuclide used is a β^+ emitter. The positron decay leads to the emission and detection of the two opposite gamma rays. In some cases, to establish a stable connection between the ligand and the radionuclide, it may be necessary to use a chemical linker [24].

Radionuclides can be produced or obtained by different methods. One of them is using a particle accelerator (as a cyclotron), where a nuclear reaction occurs and leads to the formation of the radionuclide. This type of radionuclide production has become easier and simpler during the years with the evolution of compact medical cyclotrons [26]. Another method is related to the use of a generator, where a long life parent isotope decays into a short life daughter isotope. The daughter isotope is extracted as the radioisotope to be used.

Some of the most common used radioactive nuclides used in PET are shown in Table 1.2, together with some of their properties.

Table 1.2 Physical properties of some radionuclides used in PET. Adapted from [21, 24]

Radionuclide	Physical half-life $t_{1/2}$	Maximum β^+ energy (MeV)	β^+ range in water (mm)	Main Production type
Carbon-11	20.4 min	0.96	3.9	$^{14}N(p,\alpha)^{11}C$
Nitrongen-13	9.96 min	1.2	5.1	$^{16}O(p,\alpha)^{13}N$
Oxygen-15	2.05 min	1.7	8.0	$^{14}N(d,n)^{15}O$
Fluorine-18	1.83 h	0.64	2.3	$^{18}O(p,n)^{18}F$
Gallium-68	1.14 h	1.9	9.0	$^{68}Ge/^{68}Ga$-Generator
Rubbidium-82	1.3 min	3.4	18	$^{82}Sr/^{82}Rb$-Generator

1.3.3.2. The Gallium-68 isotope

^{68}Ga is a positron emitter with a half-life of 68 minutes. It emits a 1.92 MeV positron with a probability of 89%. The remaining 11% correspond to the electron capture process (EC) [27]. Due to the disintegration by electron capture, ^{68}Ga emits gamma photons. The main single photon energies and emission probabilities are presented in Table 1.3.

Table 1.3 Energies and probabilities of the main ^{68}Ga γ-ray emissions. Adapted from [28].

Energy (keV)	Emission Probability (%)
γ -EC 578,5	0,03
γ-EC 805,8	0,09
γ-EC 1077,3	3,22
γ-EC 1261,1	0,09
γ-EC 1883,2	0,14

This isotope has properties that turn it into an excellent candidate to be used in PET. It has a good half-life, short enough to allow low radiation exposure of the patient (during

and after exam), enabling short and efficient exams, and long enough to permit efficient biodistribution in the target tissue. Its high positron emission rate also allows for a high detection efficiency.

Gallium-68 can be obtained by two different methods. The first one, being the standard method, is the Germanium-68 – Gallium-68 generator system, mentioned in Table 1.2. ^{68}Ge is the parent isotope of ^{68}Ga, with a half-life of 270.8 days (nearly 9 months) [27]. This generator system is used to easily elute and extract ^{68}Ga for the later radiopharmaceutical labeling [29, 30]. The second method, less used due to its complexity and non-rentable costs, is the cyclotron production of ^{68}Ga by a proton bombardment of a solid Zinc-68 target. The resulting nuclear reaction occurs when a proton enters and interacts with the ^{68}Zn nucleus. This interaction leads to the formation of a ^{68}Ga nucleus and the release of a neutron. The correspondent nuclear reaction can be represented as ^{68}Zn(p,n)^{68}Ga [31].

^{68}Ga interest has increased on the past years for different reasons. One of them is related to the evolution and acceptance of PET as a strong and indispensable technique for image diagnosis, with easier clinical applications. Secondarily, the previously mentioned ^{68}Ge/^{68}Ga-generators have been more available, with simpler and faster methods for the ^{68}Ga elution and later labeling into suitable PET radiopharmaceuticals. The possibility of labeling various peptide compounds with Gallium-68 has also helped for this interest growth. Subsequently, the feasible formation of stable complexes of ^{68}Ga^{3+} with different chelator types led to less complex radiolabeling methods of biomolecules. Finally, due to the simplified methods for ^{68}Ga availability and labeling methods, Gallium-68 radiopharmaceuticals have been more and more considered as viable alternatives to other isotope based radiopharmaceuticals, such as ^{18}F and ^{11}C [30, 32].

Recent studies of ^{68}Ga have been continuously showing its potential, leading to the increasing research and development of PET imaging approaches for the detection and analysis of neuroendocrine tumours [33].

1.3.4.   Nuclear Imaging in NETs

Neuroendocrine tumours usually overexpress a specific peptide kind of cell receptors, the SST. Radiotracers based on somatostatin analogues can therefore be used for tumour visualization, by using scintigraphy and positron emission tomography techniques. These approaches offer a different alternative to x-ray and magnetic resonance imaging diagnosis [34-36].

In conventional nuclear medicine, most common SST analogues used in imaging techniques for the detection and analysis of neuroendocrine tumours were usually labeled with ^{111}In and ^{99m}Tc [8, 16, 37]. More recently, ^{68}Ga proved to be an excellent peptide labeled isotope for NETs imaging with PET [38] .

1.3.4.1. The importance of Somatostatin Analogues

As it was previously mentioned, somatostatin is a peptide responsible for inhibiting the secretion of all known gastrointestinal tract hormones.[9]. It is mediated by the membrane-bound receptor SSTR, a G protein-coupled receptor, which normally exists in tissues such as the thyroid, brain, gastrointestinal tract, kidney, spleen and pancreas. However, they are abundantly overexpressed in neuroendocrine tumours, which can be taken into advantage for the neuroendocrine tumour image studies [38].

Somatostatin receptors have five different subtypes ($sst_1 - sst_5$). Only three of them, str_2, sst_3 and sst_5, have sufficiently high affinity with most of the in-hand synthetic analogues that are commercially available [37, 39]. These synthetic analogues still differ in their affinity to each somatostatin receptor, being used to detect abnormal presences of the SSTR in the different tissue cells and consequently neuroendocrine tumours [38]. However, most of them only bind with high affinity levels to the SSTR subtype 2. This affinity is sometimes not enough for an acceptable tumour detection, since the distribution and densities of the sst_2 in NETs varies [39].

The use of SST analogues has been significant relevant for the study of NETs. It allows the possibility NETs therapy, improving as well the image diagnosis [40-42].

1.3.4.2. Indium-111 labeled peptides in NETs

The radioisotope ^{111}In has a half-life of 2.8 days. It is a gamma ray emitter commonly used to perform scintigraphy or single photon emission computed tomography (SPECT) exams [8].

In these image modalities, synthetic somatostatin analogues are used, as octreotide. Octreotide based radiopharmaceuticals, such as ^{111}In-diethylenetriaminepentaaceticacid (DTPA)-octreotide, can bind to NETs cells. This radiopharmaceitucal has an affinity for the somatostatin receptor subtype 2 (sst_2), with more than 80 % sensitivities reported [8, 34]. It also has affinity, although lower, to the somatostatin receptors 3 and 5 [43]. However, the radiopharmaceutical physical properties are not good enough for the detection of small tumours. Therefore, there was a need for the research of other isotopes and approaches to take, such as the use of ^{68}Ga in PET [8, 27].

1.3.4.3. Gallium-68 labeled peptides in NETs

Recently it has been shown that PET is a more successful technique to diagnose neuroendocrine tumours [44]. The widely used radiopharmaceutical ^{18}F-FDG is currently used for the detection of a variety of tumours. FDG is a glucose analogue, allowing the detection of tumours by mapping areas in the organism where the metabolic activity of the cells is abnormally high. Despite the wide variety of options, ^{18}F-FDG has low sensitivity for the detection of tumours with low metabolic activity and slow growth rate, as in the case of most NETs [8].

The introduction of ^{68}Ga labeled peptides had a positive response in the research of new NETs detection approaches, improving imaging analysis of NETs with PET and PET/CT techniques [38]. The labeled peptides to be used in PET are based on a DOTA chelator (1,4,7,10-tetraazacyclododecane-1,4,7,10-tetraacetic acid), forming the Gallium-68-DOTA [38]. [68]Ga incorporation can be substantial, with strong bindings, even into a few nanograms of the somatostatin analogues DOTA peptides [45]. Consequently, this binding process results into high stable complexes for *in vitro* and *in vivo* studies [46].

DOTA is a universal chelator that allows the formation of stable complexes with metallic radiotracers, which includes ^{64}Cu, ^{67}Ga, ^{68}Ga, ^{90}Y, ^{111}In and [177]Lu [38]. Different DOTA based peptides can be used as somatostatin receptors PET tracers, such as [68]Ga-

DOTANOC ([DOTA^0,1-NaI^3]-octreotide), ^{68}Ga-DOTATATE ([DOTA^0,Tyr^3,Thr^8]-octreotide) and ^{68}Ga-DOTATOC ([DOTA^0,Tyr^3]-octreotide) [39]. The three different DOTA based peptides have good uptake kinetics, also due to their small size, enabling rapid binding to the SSTRs and organism clearance [32]. Both DOTATOC and DOTATATE ^{68}Ga radiopharmaceuticals have only higher affinities to the sst$_2$, while ^{68}Ga-DOTANOC can be highly specific to the SSTR subtypes sst$_2$ sst$_3$ and sst$_5$. The last is therefore reported to significantly detect more GEP-NET lesions in PET than the others [39].

Figure 1.5 shows the structures of the different labeled ^{68}Ga somatostatin analogues most used in nuclear medicine radiopharmaceuticals [32].
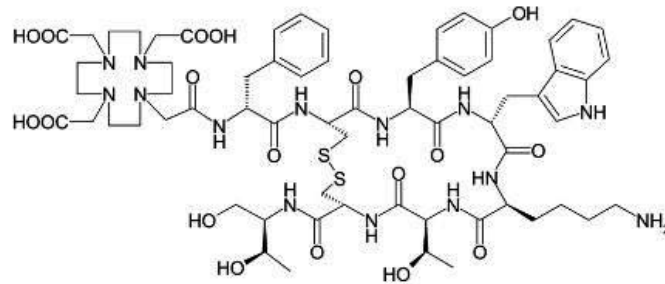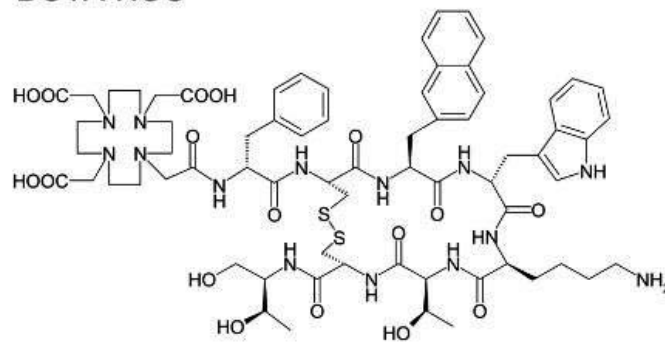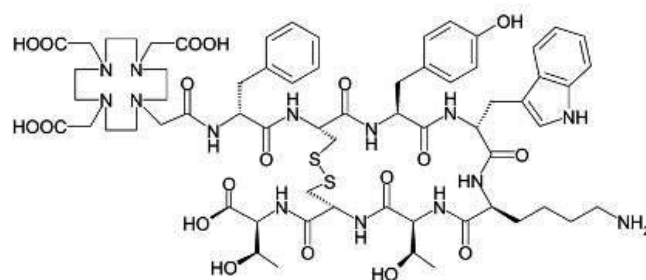
Figure 1.5 Structures of the conjugated peptides DOTATOC, DOTANOC and DOTATATE [32].

When compared to ^{111}In scintigraphy and SPECT approaches, Gallium-68-DOTA radiopharmaceuticals have been considered and proved to provide higher detection rate yields in PET, with a better tumour identification. It also has higher tumour to non-tumour radiopharmaceutical uptakes [27].

1.4.   The Cyclotron

Particle accelerators allow the production of intense beams of high energy particles that are accelerated towards a nucleus target. The resulting nuclear reactions can lead to a better comprehension of the atomic nucleus in matter, together with the study of particle penetration and artificial synthesis of matter.

A cyclotron is a cyclic particle accelerator. The accelerated particles travel in a close circular trajectory through an electric and magnetic fields, until they achieve the desired energies for target irradiation [47].

Nowadays, cyclotrons are used in facilities to produce isotopes by a charged particle bombardment into a target. The produced isotopes are later used for labeling of PET radiopharmaceuticals.

1.4.1.   Principles

In a cyclotron, an electric field must be applied in order to accelerate charged particles, in this case protons or deuterons. An electric potential difference U is applied between two electrodes, submitting the particle charge Q to an electric field force, allowing it to accelerate. Due to the electric potential, the particle kinetic energy T is given by

$$T = QU$$ Eq. 1.2

The particle charge Q travels with a velocity v, being submitted to a perpendicular magnetic field induction B. The sensed Lorentz force F_L is given by

$$F_L = Q(v \times B)$$ Eq. 1.3

This force is perpendicular to both the magnetic field B and velocity v. If the magnetic field is uniform, the path experienced by the particle will be circular. The Lorentz force

provides the centripetal acceleration that keeps the particle in a circular orbit [48, 49]. Hence, F_L is equal to the centripetal force F_p, given by

$$F_p = \frac{mv^2}{r}$$

<div align="right">Eq. 1.4</div>

where r is the radius of the circular orbit and m is the mass of the charged particle.

The representation of the charged particle moving in a magnetic field can be seen in Figure 1.6.
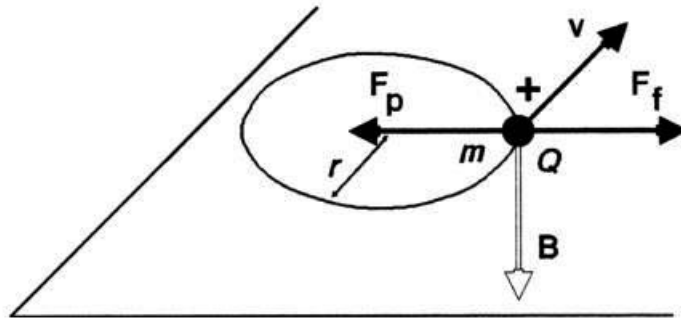
Figure 1.6 Schematic representation of a charged particle being accelerated through an electromagnetic field. F_f is the centrifugal force sensed by the charged particle as it deviates from the original trajectory [50].

The kinetic energy T of the accelerated particle can be deduced from Eq. 1.3 and Eq. 1.4, as

$$T = \frac{mv^2}{2} = \frac{Q^2 B^2 r^2}{2m}$$

<div align="right">Eq. 1.5</div>

where the kinetic energy is directly related to the ion properties (Q, m), the magnetic field induction B and the radius of the circular orbit r.

The present magnetic field is applied by an electromagnet. Two electrodes are placed between each electromagnet pole, divided into two separated cylindrical halves, as it is shown in Figure 1.7. Each semicircular part of the electrode is called "dee", given the similarity to the capital letter "D".
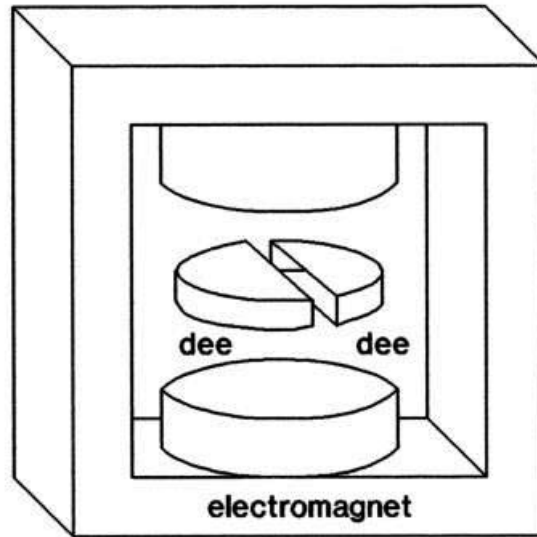
Figure 1.7 Cyclotron representation of its electromagnet with the two electrodes in each pole [50].

By relating Eq. 1.4, it is also possible to obtain the expression for the accelerated particle angular velocity,

$$\omega = \frac{v}{r} = \frac{QB}{m} \qquad \text{Eq. 1.6}$$

consequently related to particle properties (Q, m) and the applied magnetic field induction B [50].

When a charged particle is released from the center of the cyclotron, it is accelerated towards a charged dee due to the electric field sensed between the dee gap. The magnetic field is taking effect in the whole trajectory of the accelerated particle. As it enters the dee, the magnetic field forces the particle to experience a semi-circular trajectory. Once the particle finishes its path, it leaves the dee returning to the gap. It will again be accelerated, towards the other dee, where the electric field polarity must be reversed. When it enters the opposite dee, the particle experiences the same effect, traveling through a semi-circular trajectory, although the orbit radius is bigger given the higher velocity gained by the charged particle. The whole process is repeated until the particle beam has the required energy for a successful bombardment [50]. Figure 1.8 demonstrates the described process.
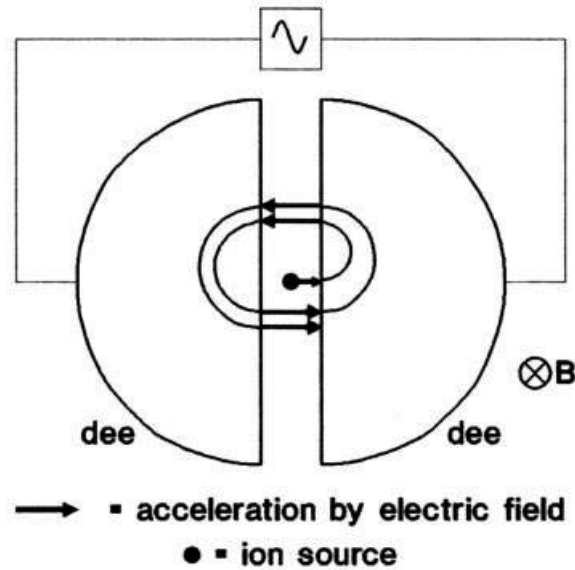
Figure 1.8 Process of acceleration of charged particles in a spiral trajectory in a cyclotron [50].

According to the theory of the ion cyclotron resonance (ICR), a particle can only be accelerated through the described process if a time-varying electric field is applied to the charged particles with the same angular velocity ω [51]. A particle can only be accelerated during its path if the polarity of the dees is changed every time the particle reaches the gap between them (i.e. the dees). For that reason, the cyclotron resonance principle is applied. As demonstrated by Eq. 1.6, the angular velocity ω only depends on the particle mass, charge and induced magnetic field. In order to satisfy this principle, the particle angular velocity ω must be somehow synched with the electric field [50, 51].

An alternating current source is therefore applied to the dees, with an angular velocity

$$\omega_E = 2\pi f \qquad\qquad\qquad \text{Eq. 1.7}$$

where f is the electric field frequency. To ensure the resonance condition, ω_E must be equal to ω. This will allow the synchronization and possibility of the particle to be accelerated every time it reaches the gap.

1.4.2. Targets

The material intended to irradiate, together with its support holder, is called target. This target material can be in solid, liquid or gas physical state, with the highest purity level possible in order to prevent undesired impurities in the final product. The target material is contained in a cyclotron target chamber, whose materials must be appropriate to resist high temperatures and pressures, also having good thermal conductivity properties.

High temperatures are sensed in the target material and in its chamber due to the beam irradiation. It is thereby necessary to implement a cooling system with a continuously water and helium flux right around the target chamber, preventing the overheating and material degradation.

In the case of liquid targets, as the most common targets for ^{18}F production, they should be composed of three main parts, also illustrated in Figure 1.9:

1. A target chamber which holds the liquid target
2. A foil window that closes the chamber in the beam direction.
3. A target body holding the chamber and window. It binds the target to the beam line, also allowing the water cooling system to be effective [52].
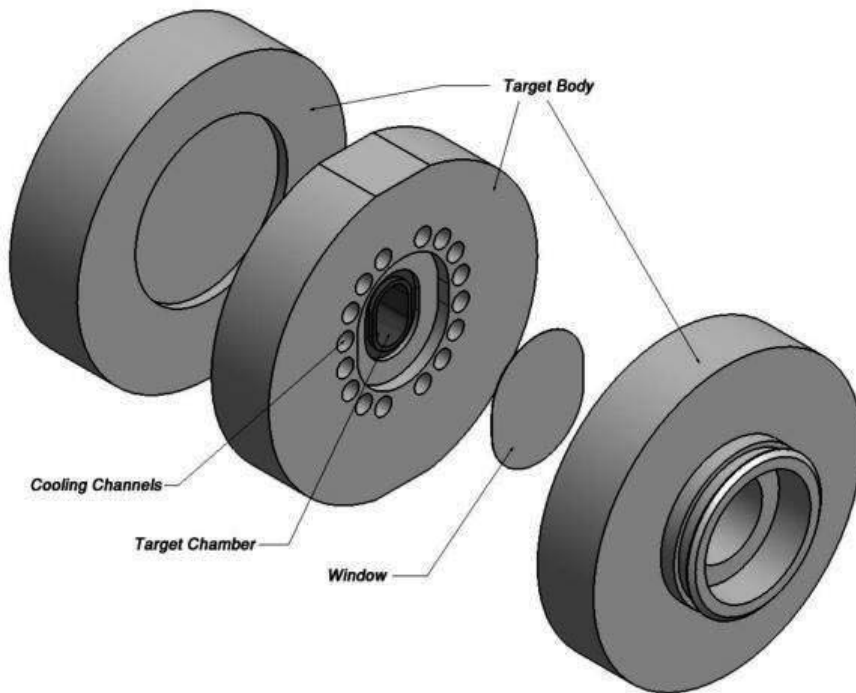
Figure 1.9 Main constituents of a liquid target system for a cyclotron [52].

1.4.3. The Traditional ^{68}Ga Production

^{68}Ga can be produced in cyclotrons by a ^{68}Zn(p,n)^{68}Ga nuclear reaction. Usually, the target chamber, made of copper backings or other materials, is electroplated with Zinc-68 in order to reach the desired thickness. Depending on the irradiation conditions and target chamber materials, a different electroplated target thickness is used. A proton beam energy of 15 MeV is reported to be more suitable to minimize radionuclide impurities, also to take the best advantage of the excitation function associated. In this case, the produced ^{68}Ga yields at the end of bombardment (EOB) can be higher than 5 GBq/μA h [31].

After irradiation, the target should be passed through a series of separation and purification steps. There are different methods for the separation of ^{68}Ga. Most common approaches follow a process which consists in:

- target dissolution in an HCl based solution;
- passing the previous solution through a retention column or cation exchange resin;
- removal of zinc and other metallic ions by a first elution step;
- ^{68}Ga extraction by a secondary elution.

These methods allow chemical separation yields of 90 %, even considering a two-step elution process.

Another important step in ^{68}Ga cyclotron production is the recovery and reutilization of the original ^{68}Zn target. The bulk solution that was eluted from the resin can be heated by an evaporation step until only salt residues remain. Secondly, the salt residues are dissolved in an HCl based solution and placed into an anion exchange chromatography column. Zinc and other metallic remains can be afterwards eluted and again used for future productions [31].

Although this methodology allows high production yields, it is a slow, complex and expensive process. Simpler and more profitable approaches should be studied.

1.4.4. A different Cyclotron ^{68}Ga production approach

Both Gallium-68 production/extraction methods have advantages, such as an easy extraction and separation of ^{68}Ga from the Germanium-68 generator, or the high yield levels obtained by the proton irradiation of a ^{68}Zn based solid zinc target in Cyclotron [29-31]. However, they also have their disadvantages. The traditional ^{68}Ga production by proton bombardment encounters important implementation drawbacks in cyclotron facilities, mainly because of ^{68}Ga target extraction difficulties and related costs. On the other hand, ^{68}Ge generators often raise problems due to limited lifetime, decrease of activity outputs and high purchasing prices. The purchasing cots associated are most of the times higher than 20.000 € per year of utilization. In order to respond to the current and future increase of ^{68}Ga use and demand, different approaches for the production of Gallium-68 should be studied and implemented.

As it was previous mentioned, ^{68}Ga cyclotron production is traditionally based on a proton irradiation of a ^{68}Zn based solid target. The fact that a solid state element is used as target implies physicochemical strategies in facilities that are difficult and complex to implement, together with the high costs associated. For an in-site simple cyclotron facility, such method is not recommended to follow. The possibility of using a based liquid element instead, as a target, could facilitate the irradiation process. In this case, the target would not need to be electroplated, having a much simpler preparation. The method would also allow easier and faster chemical processes applied in the purification and later isotope labeling.

The different approach that is studied in this work is therefore related to the possibility of producing ^{68}Ga, even in small cyclotron facilities, by a proton bombardment on aqueous solution target based on a ^{68}Zn(p,n)^{68}Ga nuclear reaction.

2. Materials and Methods

2.1. Target

This work is based in an innovative method for ^{68}Ga production in cyclotron. Selecting the target is the first fundamental step for the desired production to be successful.

The idea of using a target solution directly based on the isotope element Zinc-68 is still too premature. The costs associated with a ^{68}Zn enriched target would be too high considering that there have not been presented any test studies and results for this new approach Instead, the conducted tests were done by using natural zinc, having higher availability, lower costs and same chemistry base of ^{68}Zn. ^{nat}Zn has an isotopic composition of 18.75 % of ^{68}Zn, as Table 2.1 shows, being high enough for this work tests purposes.

Table 2.1 Isotopic composition of ^{nat}Zn. Adapted from [53].

Zinc isotope	Isotopic abundance (%)
^{64}Zn	48,63
^{66}Zn	27,90
^{67}Zn	4,10
^{68}Zn	18,75
^{70}Zn	0,62

Different zinc-based liquid solutions approaches were considered, based on zinc salts or even solid zinc dissolved solutions. The selection was focused on desirable physicochemical proprieties, behavior under irradiation conditions, activation of

constituents and expected price. This chemical interaction with the target holder materials also needed to be taken into account, being afterwards tested.

A salt solution is preferred for zinc solutions with high solubility and concentration. For this purpose, the highly available zinc chloride, zinc fluorine and zinc iodine salts were studied. Their main properties are presented in Table 2.2.

Table 2.2 – Properties of zinc chloride, zinc fluorine and zinc iodine and salts. Adapted from [54, 55].

	$ZnCl_2$	ZnF_2	ZnI_2
Molar mass	136,29 g/mol	103,41 g/mol	319,18 g/mol
Melting point	290 ^{0}C	872 ^{0}C	446 ^{0}C
Density (at 25 ^{0}C)	2,91 g/cm^3	4,95 g/cm^3	4,74 g/cm^3
Solubility in water (at 25 ^{0}C)	4,32 g/ml	Insoluble	4,50 g/ml

As Table 2.2 shows, ZnF_2 is not an appropriate salt for this work purpose. Its insolubility in water makes him a non-suitable candidate. On the other hand, $ZnCl_2$ and ZnI_2 are extremely soluble in water. However, the high molar mass of zinc iodine is undesired. When compared to a zinc chloride solution in the same conditions, a solution of zinc iodine will have a lower abundance of zinc elements. For this work purpose, the higher the abundance of zinc in the target solution, the higher the production yields will be obtained. The target was therefore decided to be based in a zinc chloride solution.

2.2. Target Chamber and Foil Window evaluation

Given the chosen target solution, target chamber and window materials needed to be studied and assessed. It was necessary to ensure high physicochemical resistance properties to a zinc chloride based solution exposure. The preliminary assumption of zinc chloride as a low pH target solution led to the research of materials capable of resisting a high corrosion environment, still fitting the physical and chemical cyclotron properties requirements [56]. Preliminary analysis showed niobium as a possible candidate, whose physical properties are indicated in Table 2.3.

Table 2.3 Niobium physical properties. Adapted from [57]

Niobium Properties	
Atomic Weight	92,9064
Density	8,57 g/cm^3
Melting Point	2468 ^{0}C
Boiling Point	4927 ^{0}C
Electrical Resistivity (20 ^{0}C)	15 $\mu\Omega$ m
Specific Heat (20 ^{0}C)	265 J Kg^{-1} K^{-1}
Thermal Conductivity	52 W m^{-1} K^{-1}

Niobium is used in a variety of applications and industries, such as cathodic protection anodes, superconductivity applications, rocket nozzles, aircrafts, sodium vapor lamps, jewelry, including as well chemical processing applications given its high corrosion resistance to different mediums [57]. More importantly, it is commonly considered as a target chamber material in cyclotron applications, widely used in ^{18}O-enriched water target chambers for ^{18}F productions [58]. Its properties are therefore highly appropriate to tolerate and fit the cyclotron conditions.

Niobium is also considered to be an excellent candidate, supporting $ZnCl_2$ solution conditions. Even with boiling temperatures and concentrations up to 70% wt (weight percent) there are unreported results of corrosion rates [57].

Despite the optimistic initial research results, corrosion resistance tests needed to be performed in the chosen target window and chamber material before cyclotron irradiations. In order to evaluate and ensure the chemical resistance of niobium to a $ZnCl_2$ acidic environment, niobium foils were obtained from Goodfellow Cambridge in England, with the properties presented in Table 2.4.

Table 2.4 Niobium foils properties from Goodfellow Cambridge.

Niobium foil properties	
Thickness	0,25 mm
Purity	99,9 %
Coil width	300 mm
Size	25x25 mm
Temper	Annealed

2.2.1. Physical study: Effect of Zinc Chloride solution to Niobium

Niobium foils were intended to be exposed to a $ZnCl_2$ environment. For that purpose, two different zinc chloride based solutions were prepared.

The first solution was prepared with a mass/solvent volume proportion of 50 g of $ZnCl_2$ salt (98% purity, supplied by Panreac) to 50 ml millipore-Q H_2O. A second solution was prepared with a similar mass/solvent volume proportion of 50 g, of the same $ZnCl_2$ salt, to 50 ml of a previously prepared 10 M HCl solution. The measured pH value of this solution in a digital meter was below the sensitivity range of the apparatus. The use of such acidic conditions had the purpose to expose a niobium foil to an extreme acidic environment, and so to evaluate the chemical resistance limitations of niobium.

A niobium foil, with an initial measured mass of 1.3825 g was dipped in the first $ZnCl_2$ solution. Another foil, with 1.3815 g mass, was dipped in the second solution (i.e., the most acidic one). Both foils were weighed in an ADA 120LE analytical balance, with a resolution of 0.1 mg. After that, they were dipped in a closed environment, deprived from oxygen, with constant agitation and temperature of 25.0 ($\pm$ 0.1) ^{0}C. In order to do so, a Grant thermostatic bath was prepared. A third niobium foil was kept aside in a closed space, without any solution exposure, to serve as a control sample.

After 40 days, both niobium foils were retrieved from the two solutions and placed in petri dishes. They were afterwards dried with a Labconco Freezone 4.5 lyophilizer, during

18 hours with a 0.024 millibar pressure and a -54 ^{0}C temperature. This helped to sublime the retained solvent in the foils. After this, the foils were again weighted before analyzed through a scanning electron microscope. They were also studied by an energy dispersive X-ray spectroscopy.

2.2.2. Scanning Electron Microscopy (SEM)

The three niobium foil samples were analyzed though a scanning electron microscopy in order to evaluate the physical differences of their surfaces.

SEM is a technique capable of nanoscale measurements and structural characterization of material surface morphology [59]. It consists on a scanning beam of electrons, with energies around 40 keV, focused on a material surface area. These electrons interact with matter, leading to the production of characteristic X-rays and consequent release of secondary electrons. These secondary electrons, only having energies of some tens of eV, are detected and used to generate an output signal of an image [60]. The equipment consists of:

- an electron gun followed by a lens system to produce and focus the electron beam
- deflection coils that determine the scanning area, depending on their current or voltage
- a detector used to collect the emitted secondary electrons from the analyzed sample

Figure 2.1 shows a common schematic structure of a SEM equipment.
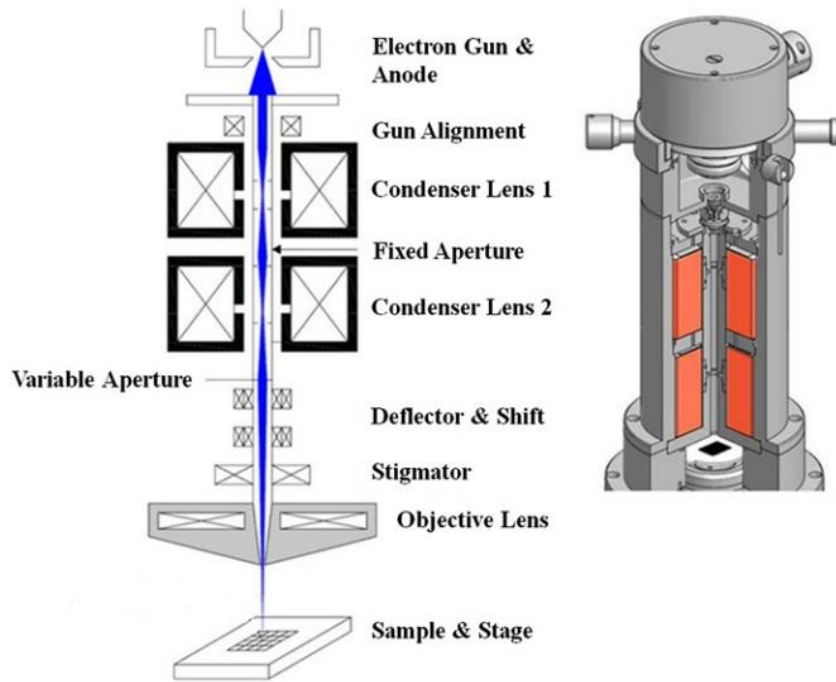
Figure 2.1 Scheme of a typical Scanning Electron Microscope. Adapted from [59].

Due to the excellent resolution and surface characterization possibilities of the technique, SEM demonstrated to efficiently evaluate the surface of the three niobium foil samples, including the control. SEM was done in Instituto Pedro Nunes (IPN), in Coimbra, with a scanning microscope Joel JSM 5310.

2.2.3. Energy dispersive X-ray Spectroscopy (EDS)

Given the possibility of element identification and characterization of the niobium samples, an Energy dispersive X-ray spectroscopy showed to be a good follow-up study after SEM.

EDS is a complementary technique to SEM that allows elemental identification, analysis and characterization of a sample surface. The SEM primary electron beam leads to a release of characteristic X-rays by interacting with the analyzed sample. The EDS system detects and processes these characteristic X-ray energies, which are unique for each element [61]. Figure 2.2 illustrates the principle of EDS.
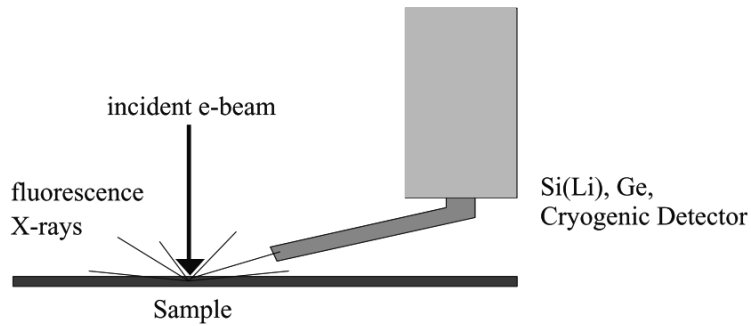
Figure 2.2 Illustration of the EDS principle [61].

An energy dispersive X-ray spectroscopy was therefore performed to the same niobium foil samples that were submerged into the zinc chloride solutions. Due to logistic reasons the EDS could only be performed one month later to the prior SEM analysis. The samples were kept in a dry place during that time, without any surface treatment. This analysis was performed in Instituto Pedro Nunes (IPN), in Coimbra, with the Oxford X-Max 60908-X020 EDS equipment.

2.3. Target Solution Transfer

In cyclotron facilities, it is necessary to use transfer lines between the cyclotron room and hot cells, for practical and radioprotection reasons. These transfer lines usually consist on polytetrafluoroethylene (teflon) tubes [62]. Teflon is a semi-crystalline polymer used in a variety of applications because of its excellent physicochemical properties, such as high resistance to corrosion and very low friction coefficient [63]. Such properties make teflon an excellent line transfer material to be used in cyclotron facilities.

Since the target solution, foreseen to be used for this work purpose, is expected to be acidic and corrosive, it is necessary to evaluate the solution effect on the line transfer materials used [56]. For that reason, two teflon tube samples were dipped, each in one of the $ZnCl_2$ solutions prepared for the previous niobium foil tests. They were submerged in 5 ml volumes for 30 days at room temperature. A control teflon sample was dipped in millipore-Q H_2O, in the same conditions. After that period, the three samples were submitted to a thermogravimetric analysis.

2.3.1. Thermogravimetric Analysis (TGA)

Thermogravimetric analysis is a thermal technique that allows the characterization of polymeric materials by studying their thermal stability conditions. It is most of the times used to evaluate a polymer material fit to a desired application, analyzing its mass degradation within a temperature range [64].

The TGA system records the sample weight loss as a function of time and temperature, within temperature ranges that can go up to 1500 ^{0}C, with low or high heating rates at a given pressure [65, 66].

The three teflon samples were first weighed and dried in a moisture analyzer scale (AND MS-70). The samples had a similar mass, approximately 10 mg each. Afterwards they were individually submitted to a thermogravimetric analyzer[2]. The system was set to have a heating rate of 20 ^{0}C/min and an end temperature of 850 ^{0}C, under a N_2 atmosphere. Data processing was performed with Proteus$^{®}$ software for thermal analysis and GraphPad Prism (version 6.02).

2.4. Gallium extraction from the target solution

Having the solution target selected, as well as the materials used in the target window, chamber and transfer lines, it is still necessary to evaluate the purification and separation of the cyclotron produced ^{68}Ga.

After a cyclotron production, the final state of the target solution cannot be readily used in the labeling process into the final radiopharmaceutical. In the end of bombardment (EOB), the target solution is still a mixture of element impurities to the labeling process. These impurities derive from the original zinc chloride solution and also from other isotope elements produced during irradiation. For this purpose, it is necessary to isolate and recover the gallium ions from the rest of the solution.

---

[2] Netzsch TA-System Controller TG 209 F3, located at the Chemistry Department of the University of Coimbra

2.4.1. Gallium extraction

Gallium, like other substances, can be retained and extracted by using resins based on ion exchange processes. Ion exchange resins are insoluble substances filled with positive or negative ions, being capable of exchanging them with the surrounding ions of a solution. A cation exchange resin swaps positively charged ions, whereas an anion exchange resin swaps negatively charged ions. The principle is therefore based on a resin R filled with ions of type A capable of exchanging them with the ions B contained in a passing solution, as shown:

$$RA + B^{n\pm} \leftrightharpoons RB + A^{n\pm} \qquad\qquad \text{Eq. 2.1}$$

This happens for a resin with a higher affinity for the ion type B than for the ion type A. The B ion is later eluted with a resin specific solution. The affinity (i.e., the selectivity) of a resin to a substance is different depending on the ions size and charge, solution concentration or resin activation method [67].

Gallium ions are in a 3+ state (Ga^{3+}). In this case, the cation exchange resin Strata-XC has been successfully used in Ga retention, with positive results [67, 68]. Therefore, we tested it, with a mass of 200 mg. Another cation exchanger resin looked promising to strongly retain gallium - the Dowex 50W-X8 [69-71]. It was tested as well. Both resins were activated with a 1 ml HCl 4M solution, followed by 10 ml of ultra-pure water.

2.4.2. Retention and Elution Activity tests

To initially evaluate the best methods for gallium extraction, prior to the irradiation tests, an experiment to study the different ion exchange resins and column methods was conducted. A $ZnCl_2$ solution with a concentration of 5 M was prepared with Sigma-Aldrich zinc chloride reagent grade (purity $\geq$ 98%) and ultra-pure water. Nearly 1.5 ml portions of this solution were mixed with small volumes of 0.6 M HCl eluate solutions from a [68]Ge-^{68}Ga generator (iThemba LABS). The goal was to simulate the conditions of an irradiated $ZnCl_2$ target solution to trap and recover the produced gallium isotopes, although with some limitations. The physicochemical differences of an irradiated solution, such as its concentration and present impurities, will be taken into account.

Additionally, the solutions of $ZnCl_2$, containing ^{68}Ga from the iThemba generator, were diluted in different volumes of ultra-pure water. Afterwards, they were passed through the resins. During the process, both initial, retained and eluted activities were measured in a COMECER® PET-dose calibrator, integrated in a COMECER® MIP1-P1 hot-cell. The statistical analysis for the resulting data was done using the GraphPad Prism software.

The methods with the best results were later applied and consequently tested for the irradiated $ZnCl_2$ target solutions.

2.5. Cyclotron Irradiation of ZnCl₂ solutions

The final steps of this work involved the irradiation of a zinc chloride solution for the production of [68]Ga. It was first necessary to prepare the cyclotron target system. After irradiation, ^{68}Ga production was analyzed.

All irradiations were performed with the IBA cyclone 18/9 cyclotron (IBA, Louvain-la-neuve, Belgium), using 18 MeV protons, at ICNAS.

2.5.1. Target Chamber and Foil Window

The target chamber used was one of the IBA 18/9 cyclotron available target chambers designed for the production of ^{18}F, with a niobium body. A target foil window was obtained from Goodfellow Cambridge, with 0.125 mm thickness and appropriate size to the available target chamber. The niobium window foil properties are described in Table 2.5.

Table 2.5 Niobium window foil properties from Goodfellow Cambridge.

Niobium window foil properties	
Thickness	0,125 mm
Purity	99,9 %
Diameter	30 mm
Temper	Annealed

The window foil is sufficiently thick to ensure pressure resistance inside the target chamber and sufficiently thin to allow target cooling by the surrounding water flow system.

Before reaching the target, the beam energy is degraded when passing through matter, which includes the water that is cooling the chamber and its target window. For a niobium foil thickness of 0.125 mm, still considering the water surroundings, the attenuated beam will have proton energies of 16.28 MeV when reaching the target solution, according to a SRIM[3] simulation. The correspondent cross section value, directly related to the probability for the nuclear reaction $^{68}Zn(p,n)^{68}Ga$ to occur, is approximately 0.4 barns[4] [72].

2.5.2. Irradiation Conditions

$^{nat}ZnCl_2$ target solutions were prepared using a Sigma-Aldrich zinc chloride reagent grade (purity ≥ 98%) diluted in ultra-pure water. The solute/solvent ratio used was 1 g of zinc chloride to 1 ml of H_2O. The target solution was injected in the IBA 18/9 cyclotron niobium target chamber with a 0.125 mm thickness niobium foil window, from Goodfellow Cambridge.

During the irradiations, the beam current was controlled and the target pressure measured. Target cooling system temperatures oscillated between 18 and 20 ^0C.

2.5.3. ^{68}Ga production evaluation

This work is based on the hypothesis of producing ^{68}Ga with a ^{68}Zn based target solution. It is therefore necessary to initially study and test the feasibility of the process, production yields and ^{68}Ga extraction. In an initially study such as this, it is more suitable to first study the similar aspects using a ^{nat}Zn solution target instead. The consequent results can be evaluated as well as the possibility of a follow-up study using an enriched ^{68}Zn salt target solution.

As previously mentioned, the isotopic concentration of ^{68}Zn in natural zinc is about 18.75 % [53]. In theory, that turns ^{68}Ga production yield by a $^{nat}ZnCl_2$ target solution

---

[3] Stopping and Range of Ions in Matter (SRIM) – software to calculate the stopping and range of ions in matter through statistical algorithms.

[4] (1 barn = 10^{-24} cm²)

irradiation 81.25 % less effective than it could become if a ^{68}Zn enriched target were to be used. It is still sufficient to study the feasibility of the foreseen production method.

Production yields were calculated from the analysis of the measured time-activity curve in the final target solution. After bombardment, the target solution was transferred from the cyclotron to a shielded hot-cell through teflon tubes. The solution activity was measured in a dose calibrator detector and recorded during time. The extrapolation of the Gallium-68 activity curve was achieved by identification of the produced isotopes within the original activity curve. The longest half-life pattern would be identified and its correspondent isotope activity curve subtracted. This process was repeated until every isotope half-life pattern was identified and consequently subtracted to the original activity curve, with no more considerable count rates results for the analysis. Non-linear regression methods were used for each subtracted curve. They allowed the identification of the correspondent isotope half-life and initial activity. This analysis was performed by using the GraphPad Prism software.

2.5.4. Spectroscopy

The irradiation of natural zinc will lead to the production of ^{68}Ga, together with other produced gallium isotopes such as ^{66}Ga or ^{67}Ga [73]. This is possible due to the different isotopic composition of ^{nat}Zn, as shown in Table 2.1. It is expected that the nuclear reactions ^{66}Zn(p,n)^{66}Ga and ^{67}Zn(p,n)^{67}Ga will occur with high production yields.

Gallium-67 ($t_{1/2}$ = 3.26 days) has characteristic gamma-ray emission energies, as showed in Table 2.6, originated by an electron capture conversion process [74]. The use of an appropriate crystal detector system can easily identify and measure the gamma emission energies [75].

Table 2.6 Emission energies and probabilities of the ^{67}Ga γ-ray decay. Adapted from [75]

Energy (keV)	Emission Probability (%)
γ-EC 93,3	39
γ-EC 184,8	21
γ-EC 300,2	17
γ-EC 393,5	5

In this work, the use of a crystal detector well allowed a semi-quantification analysis of the ^{67}Ga production, taking into account the detected characteristic γ-ray counts given by the spectroscopy system. The identification of the specific γ-rays of ^{67}Ga will prove ^{67}Ga and consequently ^{68}Ga productions, by a ^{nat}Zn target irradiation. For this purpose, the CRC®-55tW Well Counter, with a NaI crystal detector, was used.

3. Results and Discussion

3.1. Zinc Chloride as target solution

The purpose of this work was to assess the possibility of producing ^{68}Ga via a cyclotron irradiation of a zinc liquid based target. Different zinc base solutions were taken into account, and the feasibility of a zinc chloride salt solution looked promising for the given goals. The highly available zinc fluorine and zinc iodine salts were considered, but the low solubility in water of the first, and the high molar mass of the second were not suitable.

However, zinc chloride had optimal physicochemical properties for our goal. The high solubility in water (4.32 g/ml), together with its cost and availability, allow the preparation of a high concentrated zinc solution at low cost.

In terms of the irradiation process and solution impurities, the cyclotron proton bombardment of chloride does not represent a potential contaminant disadvantage or concern. According to EXFOR[5], the only chloride nuclear reaction significant on this process is ^{37}Cl(p,n)^{37}Ar. Argon-37 is an isotope with an half-life of 35 days, that decays by an electron capture process [76]. Additionally, the chlorine present in the target solution is also not an important concern. In the ^{68}Ga purification and labeling process, performed with the ^{68}Ge generator method, the use of hydrochloric acid, which contains chloride, is needed.

3.2. Corrosion Analysis on Niobium surfaces

An analysis on niobium foils that were exposed for 40 days to the zinc chloride solutions was conducted. Sample 1 was dipped in a solution composed of $ZnCl_2$ salt (50 g) diluted in H_2O (50 ml). The second niobium foil sample was exposed to a solution of

---

[5] Experimental Nuclear Reaction Data (EXFOR)

ZnCl$_2$ salt (50 g) dissolved in 10 M HCl (50 ml). After the mentioned interval of time, samples were dried and both foils were again weighed for a mass difference analysis, showed in Table 3.1.

Table 3.1 Niobium foil samples mass analysis after exposure to zinc chloride solutions.

	Sample 1	Sample 2
Initial mass (g)	1,3825	1,3815
Final mass (g)	1,3881	1,3827
Mass increase (%)	0,40	0,08

This mass analysis is in agreement with the occurrence of possible oxides formation in the substratum of the samples. The solution where the niobium sample 1 was dipped had a considerable volume of water. Within a water medium, there could be a formation of oxide complexes based on ZnCl$_2$ that remain in the substratum. Although it is low, the 0.40 % mass increase in the sample 1 is therefore suspected to be highly related to that fact. In the other hand, within a stronger acidic medium, with a low presence of water molecules as in the solution where the niobium sample 2 was dipped, the corrosion process seems to be much more passive or even nonexistent. The mass increase of 0.08 % of the second sample was considerably lower than the first. There is a probability that this sample had a slower corrosion process, with less formation of oxides complexes that could remain in the sample surface. Nevertheless, both samples presented very low differences between their final and initial masses, possibly revealing slow corrosion processes.

These initial findings needed to be further confirmed. The scanning electron microscopy performed was foreseen to be an important analysis to corroborate these initial results.

3.2.1. SEM on Niobium samples

The scanning electron microscopy analysis revealed the reason for the mass increase in samples 1 and 2. A control sample was first scanned and studied for comparison.

In Figure 3.1 it is possible to see a clean and smooth niobium foil surface, having a common straight scratch behavior.
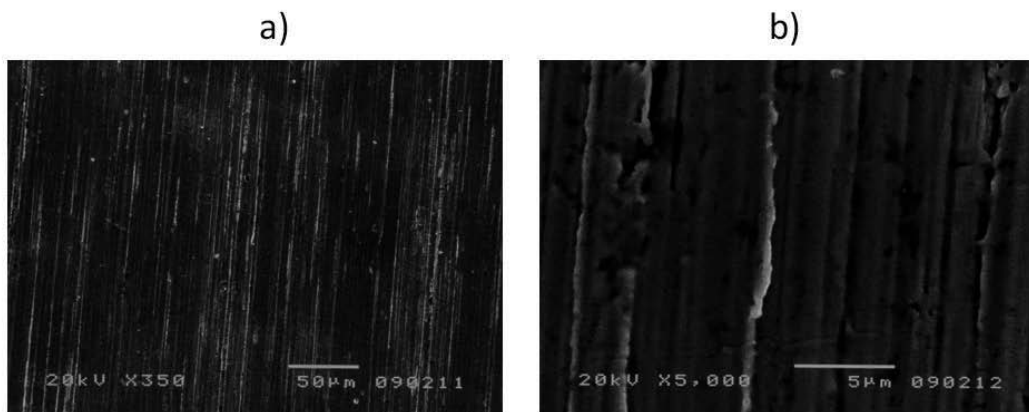
Figure 3.1 SEM scans on the niobium control sample with lower (a) and higher (b) zooms.

The SEM analysis on the niobium samples 1 and 2 showed a different surface behavior than the one seen in the control sample, as it can be seen in Figure 3.2 and Figure 3.3.
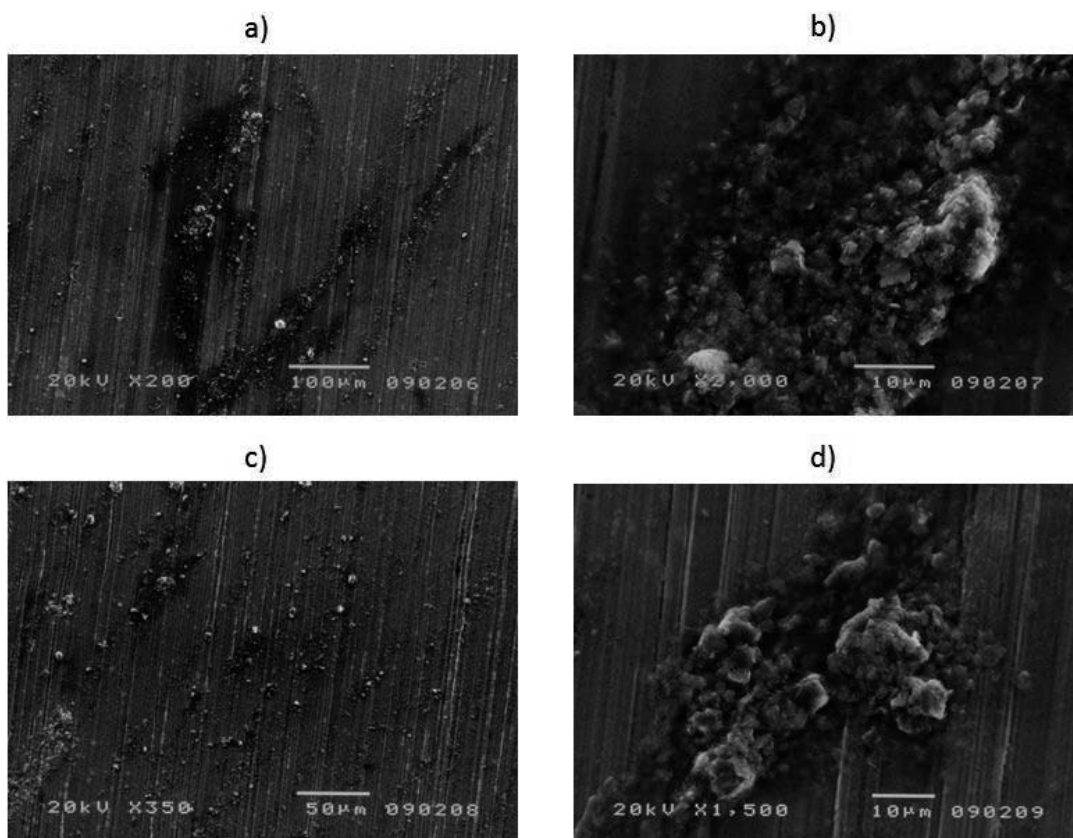
Figure 3.2 SEM analysis on sample 1, dipped in a solution of $ZnCl_2$ salt (50 g) diluted in H_2O (50 ml) during 40 days. b) and d) correspond to zoomed areas of a) and c) respectively.
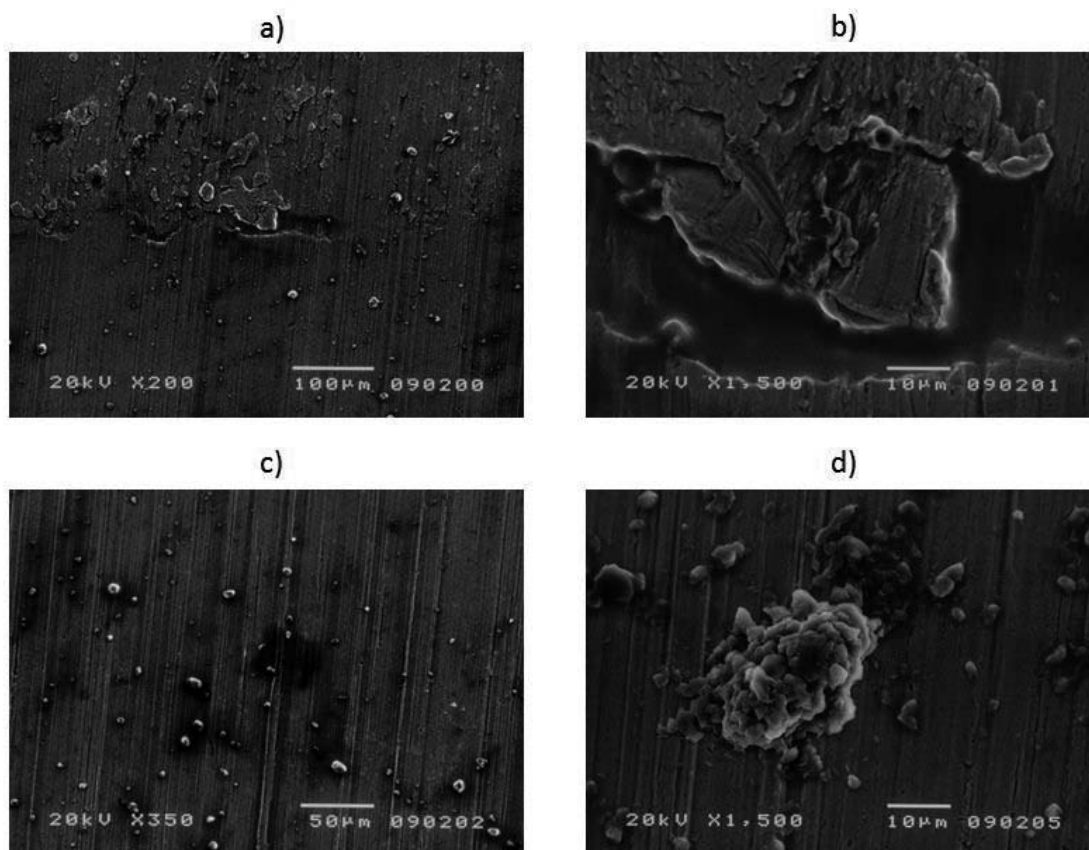
Figure 3.3 SEM analysis on sample 2, dipped in a solution of $ZnCl_2$ salt (50 g) diluted in 10 M HCl (50 ml) during 40 days. b) corresponds to a zoomed area of a).

Both samples 1 and 2 showed the same behavior pattern, apparently with a deposition of molecular aggregates around the niobium foil surfaces. The mass increase in both samples previously mentioned, is therefore related to the deposits formed during the exposure of the niobium foils to zinc chloride solutions. These aggregates are mostly related to the solution salt depositions as well with the probable formation of niobium oxides.

During SEM, it was also possible to see fewer and more structured aggregates in the foil surface of sample 2 than in sample 1. In the second sample, the phase separation seems to be spread by larger areas with different exfoliation-like patterns. This supports the information given by the mass difference analysis in the samples, where the mass increase in sample 1 was higher than the mass increase in sample 2. It also confirms the theory of a slower and less probable oxide formation in stronger acidic environments as the solution where sample 2 was dipped. This solution had a lower pH than the solution where sample 1 was exposed.

Although other studies shall be performed to better explain the corrosion mechanism in both samples, the mass analysis coupled with SEM helped to justify that most probably the acid media has an important role on the formation of a passive region. Another support for this hypothesis is the pourbaix diagram of a niobium-water system at 25 ^{0}C, represented in Figure 3.4.
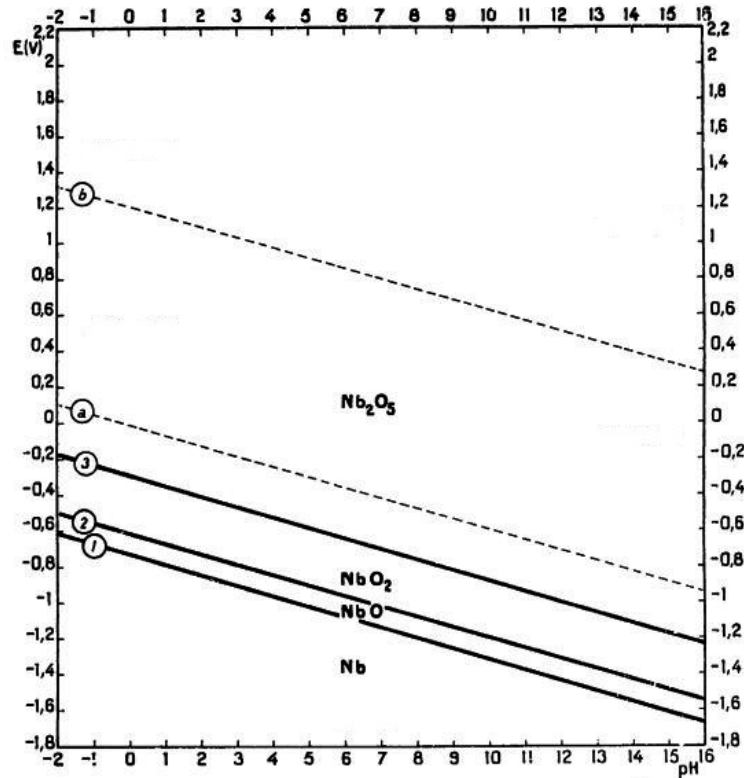
Figure 3.4 Potential-pH equilibrium diagram for the niobium-water system at 25 ^{0}C. Adapted from [77].

A pourbaix diagram is a representation of the Nersnst equation, relating a material electrochemical potential with the medium pH dependence. In these diagrams, different regions of stability can be seen [78]. The first and most stable region is called immunity, where the metal is considered to be thermodynamically stable without any corrosion occurrence. The second region, called corrosion, happens when dissolution and corrosion of the metal in the medium occurs. The passivity region, being the third, happens when the metal reacts with the medium compounds, within a corrosion process, up to a point the metal surface is covered with produced passive layer, preventing further corrosion to occur [77]. The presented pourbaix diagram, although not clearly showing the different stability regions, demonstrates that with a lower pH value the electrochemical potential needed for

oxides to occur in niobium is superior that with higher pH values. Therefore, in this system, a more acidic medium prevents the formation of oxide complexes in the metal surface with better results, slowing the corrosion process. This fact supports the reported mass increase differences in the niobium sample 1 and 2, as well as the fewer aggregate structures observed during the SEM analysis in the second niobium sample, when compared to the first. Despite the solution medium systems being different from the one considered in the pourbaix diagram, the approximate inductions are viable.

Nevertheless, it is still important to explain that both samples had very few aggregates, only seen with SEM. Furthermore, the selected SEM scans represent the less clean surface areas of the niobium samples. Although oxidation is related to the chemical corrosion process, none of the niobium foil samples showed a significant destructive corrosion in their surfaces. It is an important feedback to support a high physicochemical resistance of niobium to the corrosion influence and induction of zinc chloride solutions, even with a long period exposure.

Given the SEM results, an elemental analysis on the samples was indicated. An energy dispersive X-ray spectroscopy was made as a follow-up study.

3.2.2. EDS on Niobium samples

The energy dispersive X-ray spectroscopy on niobium foil samples 1 and 2 was made a month later to the prior SEM. EDS analysis helped to identify the elemental composition of the aggregates seen in SEM.

Figure 3.5 shows a SEM scan of an area surface of the niobium sample 1 (a), together with the EDS element spectrum of two different spots (b and c). The element characteristic x-ray spectrum shown in (b) indicates a high presence of zinc and chloride elements from the salt solution that reacted with the niobium foil surface, forming structural complexes seen in (a).

The same complex formation behavior can be seen in the niobium sample 2, as SEM and EDS analysis on Figure 3.6 shows. These complexes have clearly evolved rapidly during the time between the previous SEM and the later EDS analysis. It showed the acceleration of the corrosion process in the niobium samples after exposure to zinc chloride solutions, when the foils were put in a normal environment with air contact. At air,

the formation of electrochemical cells is much faster and easier in the surface of the niobium samples. On the other hand, the solubility of oxygen in the solution is lower, leading to a slower corrosion process compared to when the metal samples contact with air.

a)

b)

c)
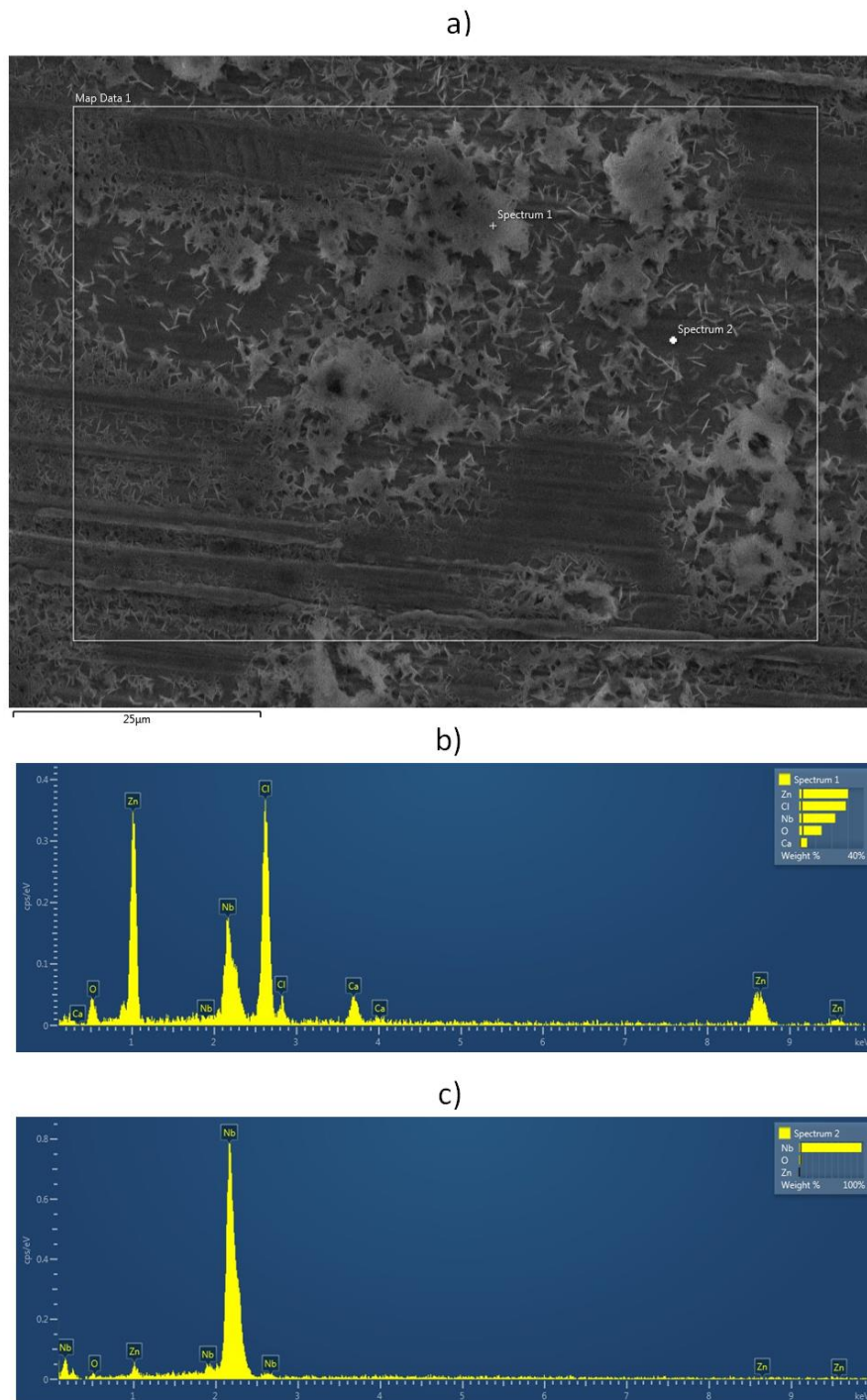
Figure 3.5 SEM scan to the niobium foil sample 1 (a) and EDS element spectrum of aggregate (b) and a clean (c) spots.

a)

b)

c)
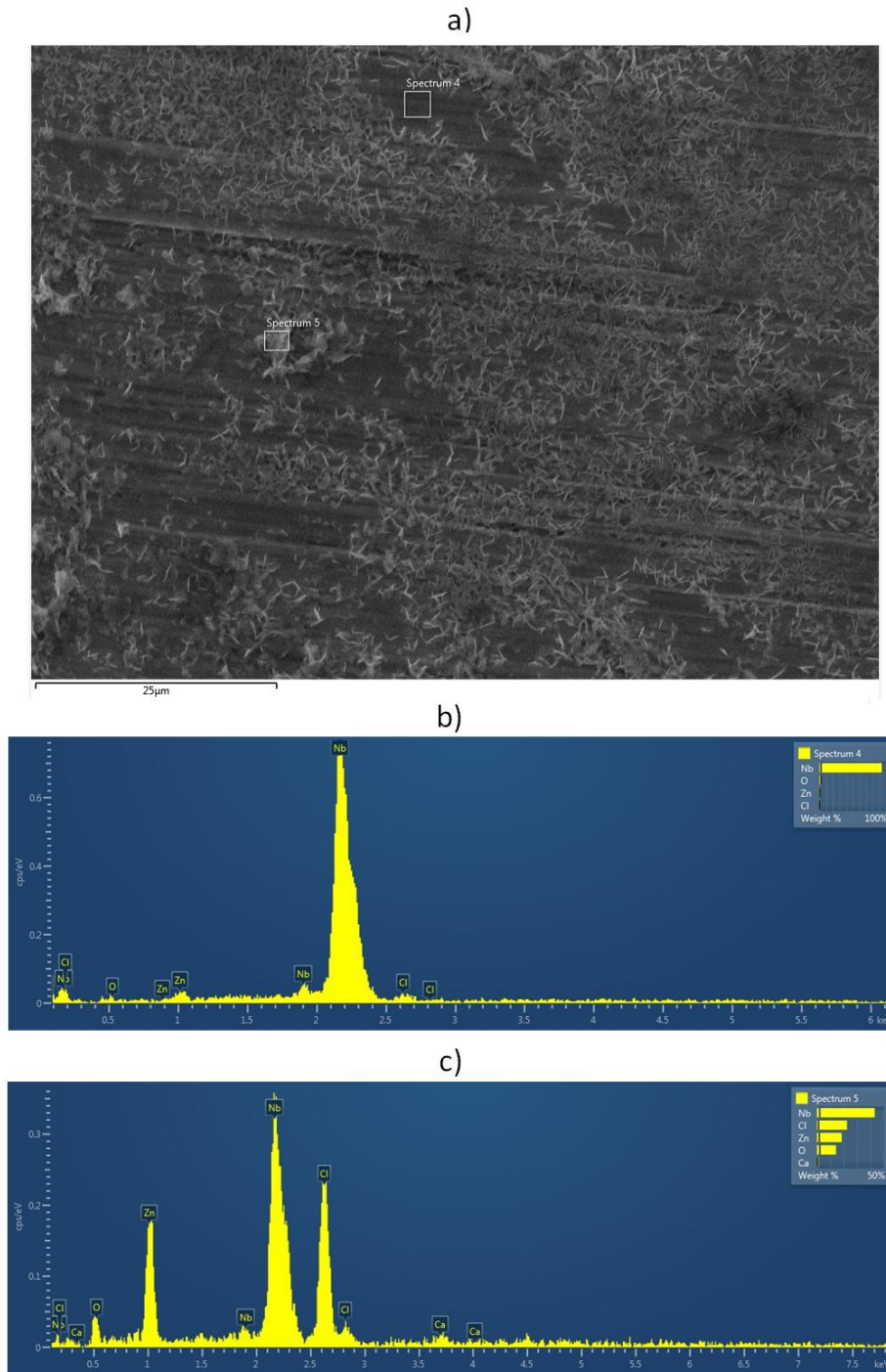
Figure 3.6 SEM scan to the niobium foil sample 2 (a) and EDS element spectrum of clean (b) and an aggregate (c) spots.

EDS also allows a mapping elemental characterization. The sum of every pixel spectrum, which gives the element most present, gives the possibility of an element map of an image scan, as Figure 3.7 demonstrates. The niobium sample 1 element maps of niobium (a), chloride (b), oxygen (c), calcium (d) and zinc (e) were found, and summed into

a reconstructed element map (f). It clearly shows the prevalence of niobium and chloride elements present in the surface of a scanned area of sample 1. When compared to the SEM image, the presence of chloride coincides with the presence of surface aggregates. On the other hand, the presence of niobium coincides with the clean surface areas. Figure 3.8 demonstrates this comparison.
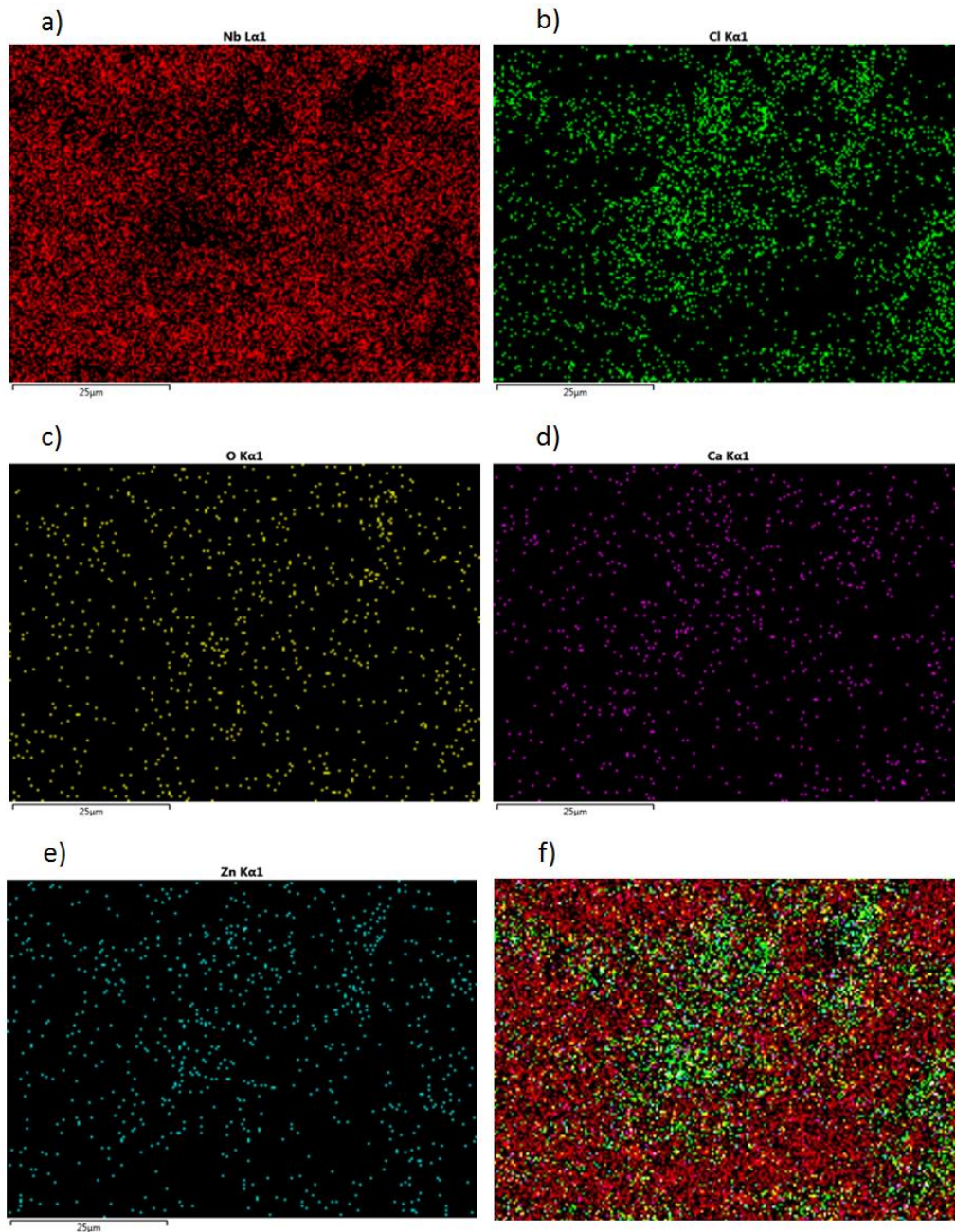
Figure 3.7 Element map of an EDS scanned area of niobium sample 1. Niobium (a), chloride (b), oxygen (c), calcium (d) and zinc (e) maps are shown. The sum of the 5 element maps forms the reconstructed map (f).
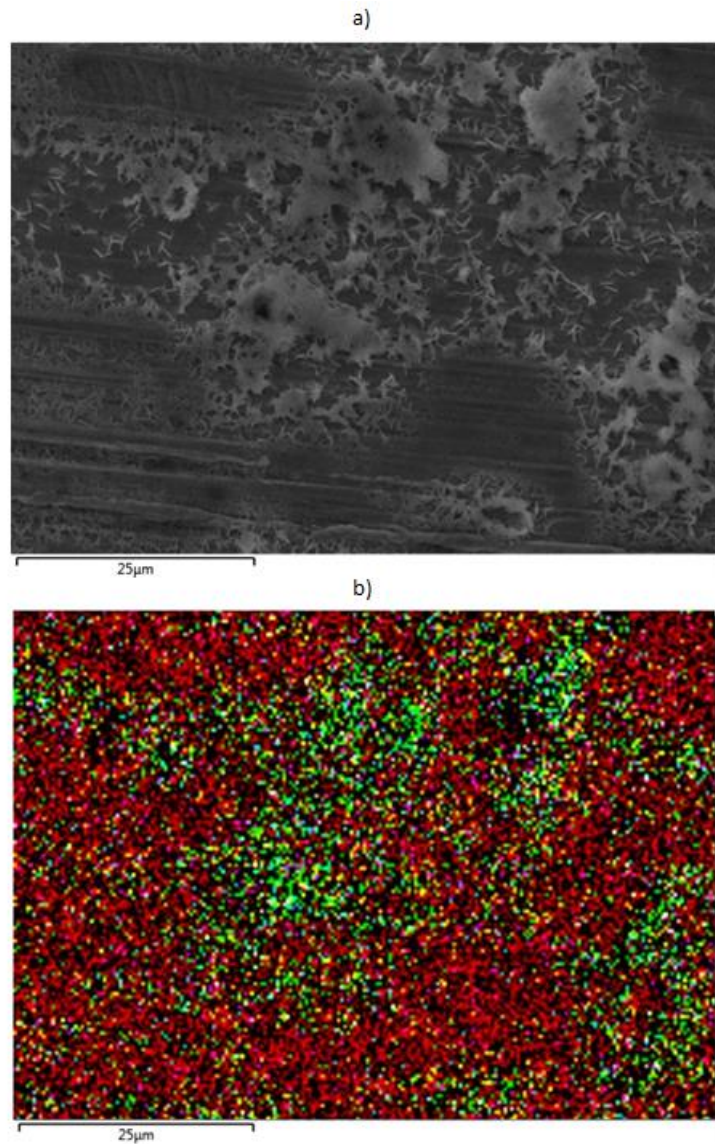
Figure 3.8 SEM scan on a surface area of the niobium sample 1 (a) compared to the
correspondent EDS reconstructed element map (b).

Another evidence of the prevalence of chloride elements in the chemical complexes
seen in the surfaces of both niobium samples is evident in Figure 3.9. In this case, blue
pixels correspond to the presence of a higher chloride spectrum and the red pixels to the
presence of a higher niobium spectrum. Less evident are the zinc, oxygen and calcium
elements represented by the colors green, purple and yellow, respectively.
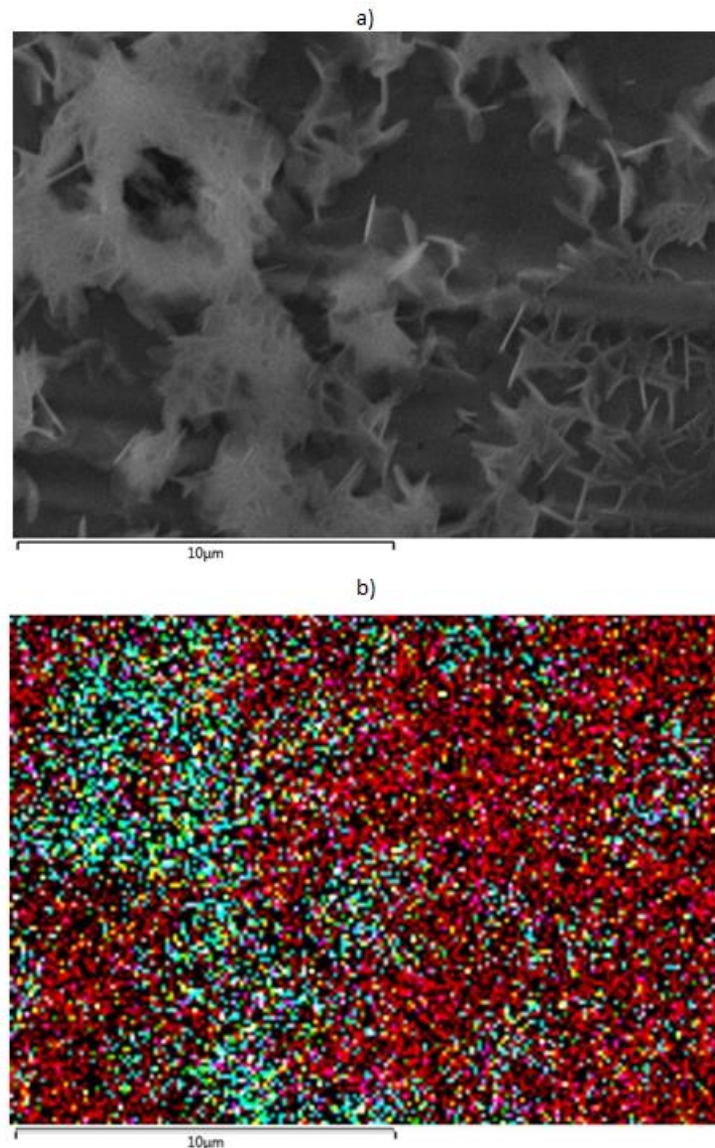
Figure 3.9 SEM scan on a surface area of the niobium sample 1 (a) compared to the correspondent EDS reconstructed element map (b).

Although they are less concentrated, the presence of oxygen elements within both samples supports the existence of oxide elements. The acceleration of the corrosion process observed in both samples, during the time passed between the SEM and EDS analyses, can be related to the exposure of the niobium samples to air. The oxygen presence in air, within a considerable humid environment, allows the formation of thin water layers in the surface of the metallic samples, where the air oxygen is fixated. The oxygen is consumed, leading to the formation of weaker thermodynamic stability points in the sample, prospective to corrosion occurrence.

The identification of calcium elements in the EDS spectrum analyses was not expected. Nevertheless, its presence can be related to different reasons. The flask materials used during the thermostatic bath of the niobium samples could still have impurities that were not completely washed during the initial cleaning process. It could also be due to sweat, since human glands still secrete small concentrations of calcium [79]. When hold, the niobium foil samples could have been in contact with the sweat present in the hands palm. Yet, the most suspected cause is water. The millipore water used to prepare the zinc chloride solutions could have calcium impurities due to the ion exchange columns in the water purification system, probably needed to be replaced.

EDS analysis revealed an important element characterization of the niobium samples. Although the chemical species of the aggregates observed were not identified, the presence of chloride and zinc is clearly related. The identification of oxygen elements in both samples spectra, together with the information of the previous analysis, indicates the formation of oxides. Consequently, it shows the existence of corrosion during the time until EDS was performed. Moreover, the air exposition consequences on the corrosion acceleration of the samples revealed that the niobium target holder, foreseen to be used in the cyclotron irradiations, should be thoroughly washed and cleaned after each irradiation, preventing oxide formations.

Ultimately, the mass, SEM and EDS analysis revealed a high physicochemical resistance of niobium to zinc chloride solutions. The niobium samples were submitted to extreme conditions, being exposed to acidic environments during 40 days. They were not even washed and cleaned during that time. Yet, the followed mass and SEM analysis only showed low mass increases, with little formation of aggregates in the samples surfaces. When exposed to air, the corrosion process was significantly accelerated, as demonstrated by the EDS. Within cyclotron conditions, niobium is expected to even better resist target solution conditions. The zinc chloride exposure will be much smaller and the target chamber thoroughly cleaned after each irradiation. The contact with oxygen will also be minimal. Hence, niobium is highly suitable to be used as target chamber and window materials to support a zinc chloride target solution.

3.3.   Degradation analysis on teflon - TGA

The thermogravimetric analysis on the chosen material for the transfer lines of the target solution showed positive results.

Three teflon samples were considered in this analysis, as described in section 2.3.1. The control sample was the one dipped in millipore-Q water. The teflon sample 1 was exposed to a 5 ml of a $ZnCl_2$ solution with 50 g of $ZnCl_2$ dissolved in 50 ml of millipore-Q H_2O. The teflon sample 2 was dipped in 5 ml of a solution composed on 50 g of $ZnCl_2$ dissolved in 50 ml of 10 M HCl. The resulting TGA graphic of the three samples is shown in Figure 3.10, where the mass lost ratio is given in function of temperature.
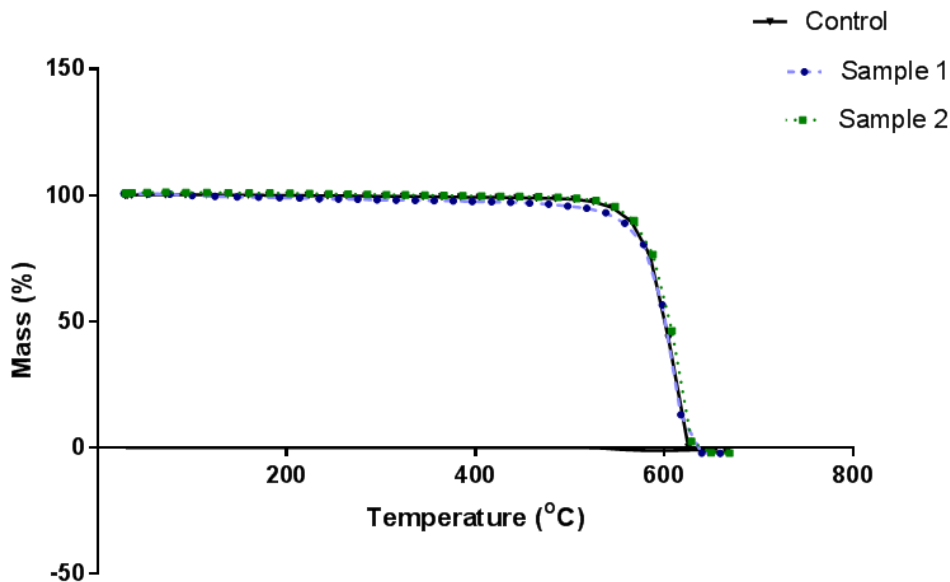
Figure 3.10 Thermogravimetric graphic of the three teflon samples, one used as control.

An analysis of the first derivative curve of the TGA (DTG) was later performed, represented by Figure 3.11. The DTG curve describes the mass loss rate with the degradation temperature (dm/dT), allowing the determination of the temperature in each transition segment of the TGA curve. It relates the inflection of the transition profile of the sample, easily showing weight loss rate changes that cannot be readily seen in the TGA curve [80, 81]. The DTG minimum gives the maximum mass lost rate at a given temperature.
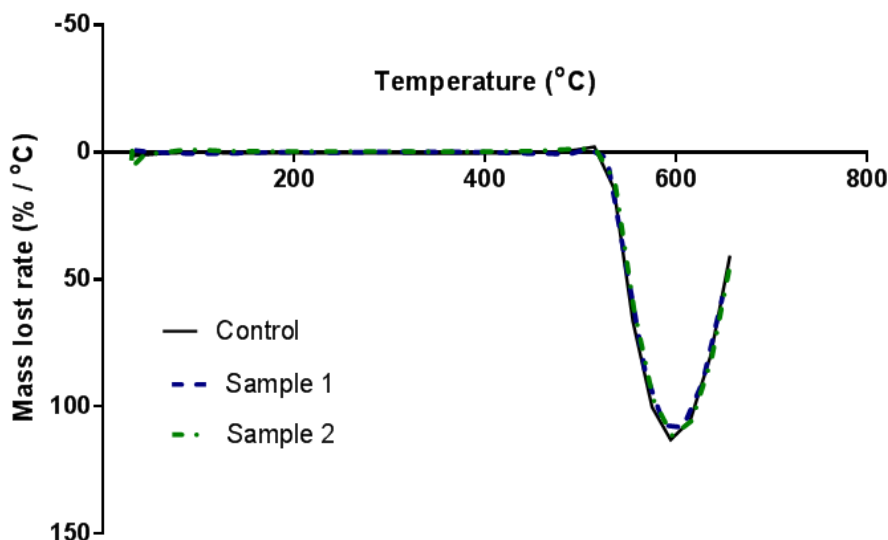
Figure 3.11 First derivative of the TGA sample curves.

The analysis revealed similar behaviors of samples 1 and 2 compared with the control, in the TGA and DTG results. The total mass loss of the three samples was registered as well as the temperature of maximum mass lost rate (corresponding to the first derivative minimum of the TGA graphic curve). The results are presented in Table 3.2.

Table 3.2 Total mass lost and maximum mass lost rate correspondent temperature of the TGA samples.

	Total mass lost (%)	Temperature of maximum mass lost rate (^{0}C)
Control sample	101,85	605,8
Teflon sample 1	102,55	609,1
Teflon sample 2	102,41	611,9

The obtained results presented in Table 3.2 show the consistency of the similar results of the TGA study on the three samples. The total mass lost, although liable to a small error, showed no presence of residues at the end of TGA. This proves the purity of the teflon material used. Furthermore, the proximity of the registered temperatures for maximum mass lost rate evidences the same material degradation pattern with temperature observed in the TGA and DTA curves, within all samples.

Teflon was therefore found to safely resist the zinc chloride solution conditions, in order to be used in the path between the cyclotron and the hot-cells, as the transfer line material of the target solution.

3.4. ^{68}Ga preliminary column tests

The elution solution from the ^{68}Ge-^{68}Ga generator of 0.6 M HCl was diluted in water. Different portions were afterwards mixed with small volumes of a 5 M ZnCl2 solution. The resulting solutions were used to test the columns adsorption for ^{68}Ga ions. The results are presented in the graphic of Figure 3.12. Different dilution concentrations of the solution that passed through the columns were used in the different tests. The best results were obtained with the cation exchanger Dowex 50W-X8 resin, prepared with a resin mass superior to 400 mg in each trial, with a positive ^{68}Ga adsorption of 92.83 ± 1.86 %. The second best result was obtained with Strata-XC, with 200 mg resin mass, with a ^{68}Ga adsorption of 85.01 ± 9.23 %.
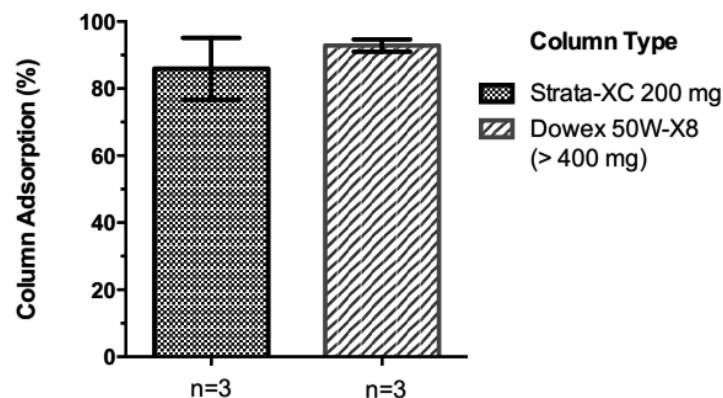
Figure 3.12 ^{68}Ga adsorption in the ion exchange resin types Strata-XC and Dowex 50W-X8.

The solution that passed through the Dowex resin columns consisted on 1.5 ml of a 0.025 M HCl dilution solution containing the ^{68}Ga mixed with 1.5 ml of a 5 M ZnCl$_2$ solution dissolved in 16 ml of ultra-pure water.

In order to better evaluate the use of the Dowex resin for ^{68}Ga retention, additional studies were performed. Besides from the diluted solution, the resin mass should also

influence the gallium retention. To study this influence, different prepared resin masses were tested to retain ^{68}Ga, having obtained the results summarized in Figure 3.13.
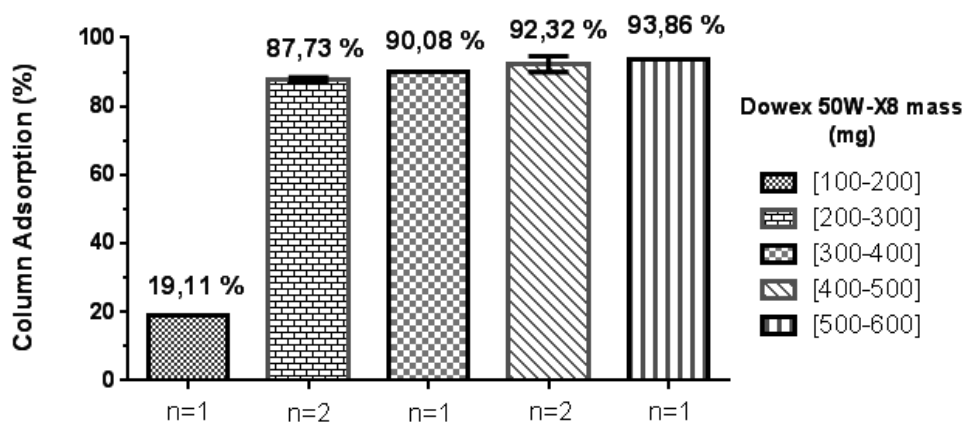
Figure 3.13 Dowex 50W-X8 ^{68}Ga absorption depending on the resin mass used.

Mass retention tests revealed positive results for resin masses superior to at least 200 mg, with a ^{68}Ga retention superior to 87 %. From there, an increase of the resin amount in the column resulted in higher adsorptions, although with smaller differences in the results, as shown in Figure 3.13.

Given that the best results were obtained with the Dowex 50W-X8 resin, gallium extraction tests were performed with it, using a 3.5 M HCl elution solution, with a volume of 3 ml passing through the column. The study outcome was found to be very positive, with a reported ^{68}Ga deabsorption of 94.25 ± 5.06 % (n=8).

3.5. Cyclotron irradiation of a ZnCl₂ solution

In total, seven irradiation tests of zinc chloride solutions were done. During each trial, several parameters were changed in order to achieve the best conditions and results. Some of the improvements were a higher target stability inside the cyclotron, the assessment of fast and appropriate transfer of the irradiated solution to a hot-cell and higher production yields.

In each irradiation, the most important and significant produced isotopes with a β^+ decay type were found. The goal was to identify, within the production time-activity curves, half-life patterns of the produced isotopes and their production yields, such as the ^{68}Ga.

3.5.1. Radionuclide identification and quantification

After assessing the appropriate stability conditions in the cyclotron during the first irradiation tests, the time-activity curve of the ^{68}Ga was found, together with the other produced isotopes.

The third production test had a cyclotron beam with an integrated proton current of 1 μA h targeted to a $ZnCl_2$ prepared solution, with 2.0 ml of volume. Figure 3.14 shows the total time activity curve measured of the final solution, when it was transported into the CRC®-55tW dose calibrator. The count rates were measured in mCi and recorded during a period of 23 hours, with a time lapse of 2 minutes in each measurement. Error bars are represented in some of the data, being 10% of the measured values.
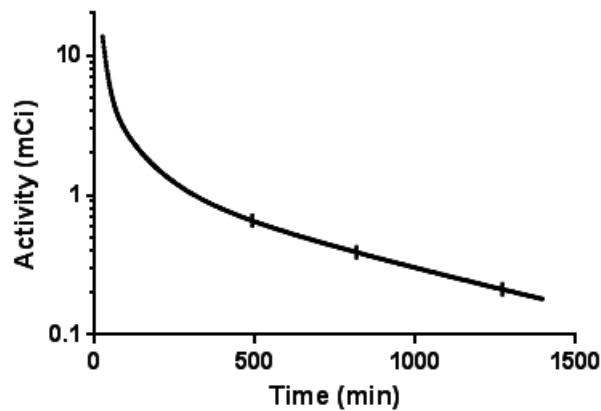
Figure 3.14 Recorded count rates (logarithmic scale) of the third cyclotron production using a $ZnCl_2$ solution.

The extrapolation of the half-life patterns of the produced isotopes was afterwards conducted, with the results presented in Figure 3.15.
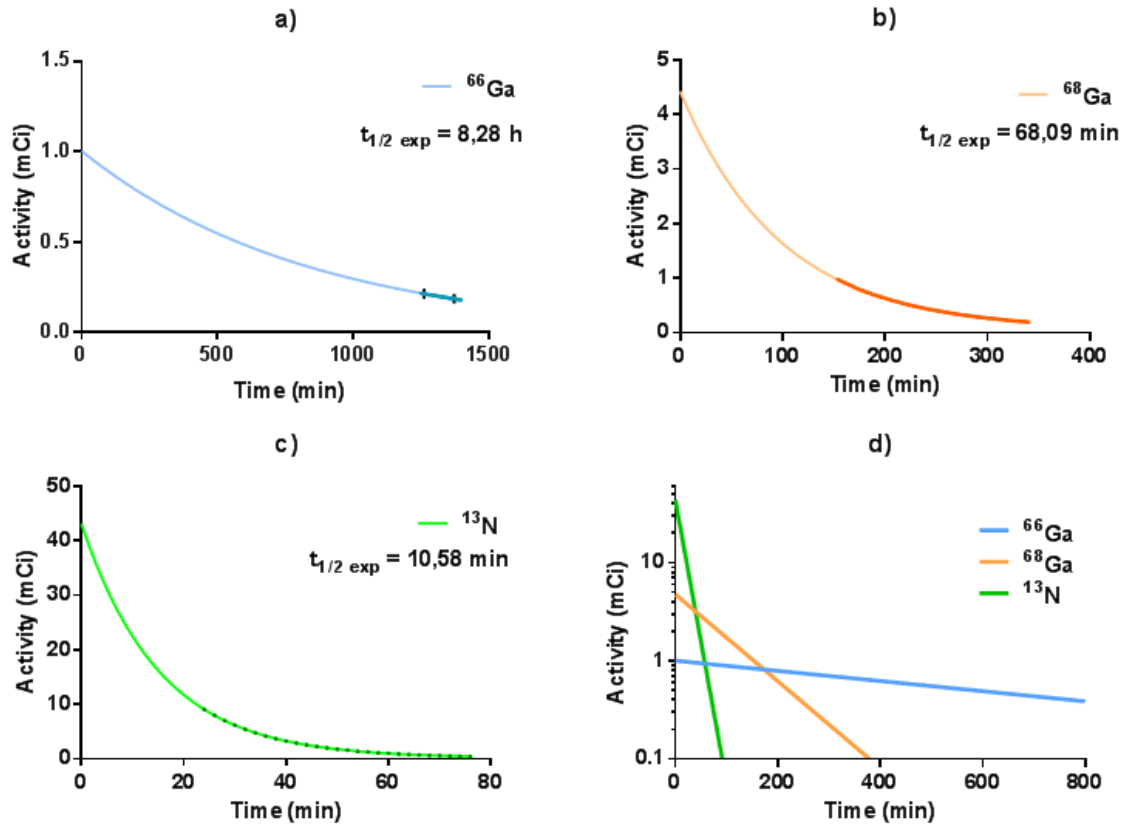
Figure 3.15 Non-linear regression curves, with the considered data of the produced isotopes ^{66}Ga (a), ^{68}Ga (b) and ^{13}N (c). Representation of the three time-activity curves of the identified isotopes (d).

The identified gallium isotopes are mainly produced by the nuclear reactions ^{66}Zn(p,n)^{66}Ga and ^{68}Zn(p,n)^{68}Ga. The used liquid target has also a high concentration of water, rich in oxygen. Since the main oxygen isotope present is ^{16}O, ^{13}N can be highly produced through the nuclear reaction ^{16}O(p,α)^{13}N. The high presence of ^{13}N in the final solution is therefore explained. All the identified isotopes decay by positron emission. Their theoretical half-life periods are summarized in Table 3.3, compared to the experimentally found.

Table 3.3 Experimental and theoretical half-life values of the produced isotopes [66]Ga, ^{68}Ga and [13]N.

	Experimental $t_{1/2}$	Theoretical $t_{1/2}$
[66]Ga	8,28 ± 1,03 h	9,3 h [82]
[68]Ga	68,09 ± 0.28 mins	68 mins [31, 82]
[13]N	10,58 ± 0.03 mins	9,9 mins [21]

As observed in Table 3.3, the experimental and theoretical half-life values of the identified isotopes are clearly proximate, although there is a considerable error when analyzing multiple phase decays. The range of the standard deviation for the [66]Ga half-life period found is due to insufficient data recorded and considered for the analysis. Since this isotope has a longer half-life, the data acquisition should be done for a longer period, in order to reduce the standard deviation error. [68]Ga production yield was calculated to be 163.73 ± 16.40 MBq (4.425 ± 0.44 mCi) at EOB.

The followed irradiation test had the purpose to target higher beam currents to the zinc chloride solution, in order to achieve higher production yields. A solution volume of 1.6 ml was injected in the target chamber. The stability of the target pressure in cyclotron, achieved by the smaller solution volume injected, allowed the irradiation with a proton beam integrated current of 6 μA h. As before, the decay rate of the final solution was recorded, in this case during a 25 hour period with the CRC®-55tW dose calibrator. The extrapolation of the time-activity curves of the produced isotopes was later performed. The analysis results are presented in Figure 3.16.
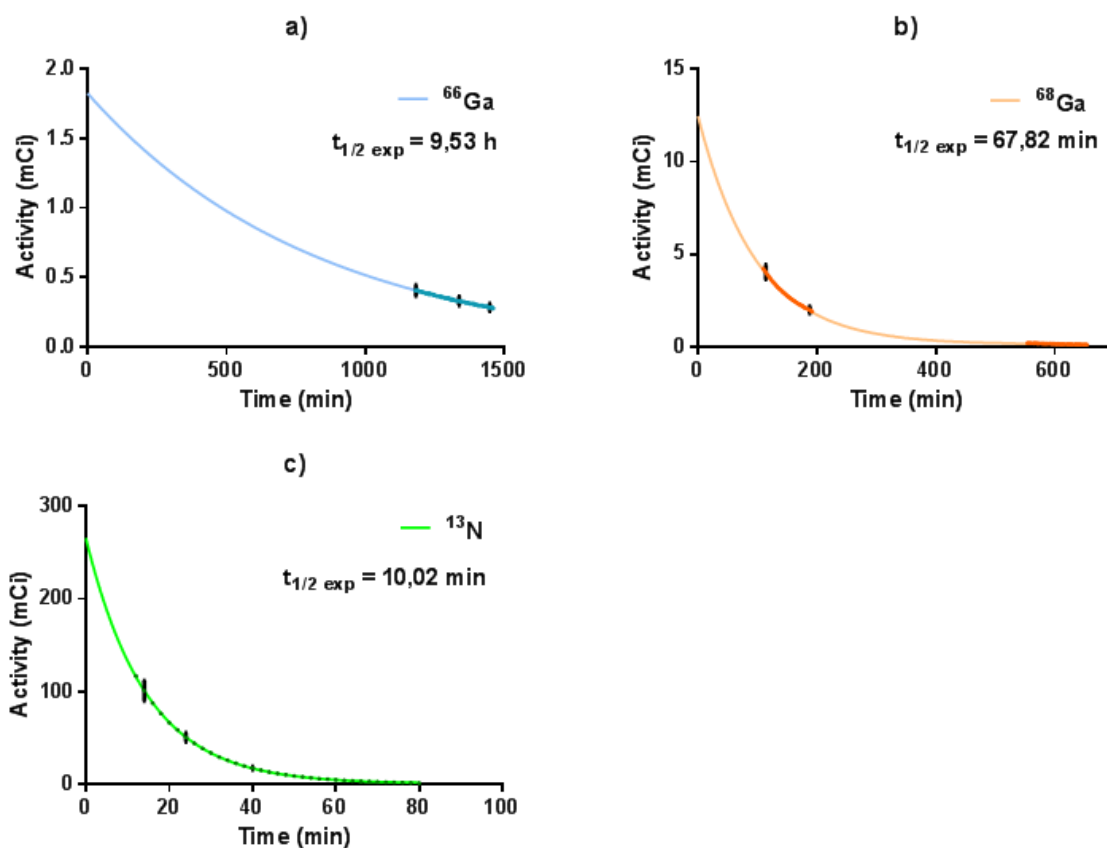
Figure 3.16 Non-linear regression curves, with the considered data of the produced isotopes ^{66}Ga (a), ^{68}Ga (b) and ^{13}N (c).

The experimentally half-life values found are still very proximate to the theoretical ones, mentioned in Table 3.3. ^{68}Ga production yield was found to be 461.76 ± 46.62 MBq (12.48 ± 1.26 mCi), for a $t_{1/2\,exp}$ = 67.82 ± 0.50 min.

3.5.2. Gallium retention evaluation

After identification of the produced isotopes and ^{68}Ga yields assessment, the purification process needed to be tested. The final solution needs to pass through a purification step, in order to separate the gallium ions. For this purpose, the final solution was passed through an ion change resin, the Dowex 50W-X8, since it showed the best retention results. Another reason for this resin to be considered for this final step is its capacity to individually separate and extract zinc and gallium ions with different elution steps [83]. It makes the Dowex 50W-X8 an excellent candidate for follow-up studies.

Therefore, a final irradiation was conducted with similar conditions as the one before, with an integrated current of 6 μA h during 30 minutes. The same concentration and volume conditions for the zinc chloride target solutions were kept. The irradiated target solution, diluted in 43 ml of ultrapure H_2O, was afterwards passed through the resin column (mass = 460 mg), with an approximate flow of 2 ml/min. Thereafter, the column was placed in the CRC®-55tW dose calibrator. The decay rate was recorded during 40 hours, started 68 minutes after EOB.

Focusing on the gallium isotopes ^{66}Ga and ^{68}Ga, a half-life extrapolation analysis was conducted. The non-linear regression results showed half-life values of 9.5 ± 0.2 hours and 67.4 ± 2.9 mins, with an initial production yield of 0.97 ± 0.10 mCi for ^{66}Ga and 2.59 ± 0.28 mCi for ^{68}Ga.

The resulting waste from the column retention step was also analyzed, in the same way as before, with the COMECER® PET-dose calibrator, integrated in COMECER® MIP1-P1 hot-cell. The data recording started 92 minutes after EOB. In the analysis, no gallium half-life patterns were identified. This corroborates the high absorption properties of the Dowex resin to gallium.

Additionally, the Dowex resin and waste were submitted to a spectroscopy analysis, 4 days after irradiation. The goal was to evaluate the presence of ^{67}Ga within both samples, since its half-life is still suitable ($t_{1/2}$ = 3.26 days) [75]. Its characteristic γ emission energies and probabilities were shown in Table 2.6.

The Dowex resin and a 1 ml sample of the waste solution were separately analyzed in the CRC®-55tW Well Counter, during 60 seconds of counting. The resulting spectra are presented in Figure 3.17.
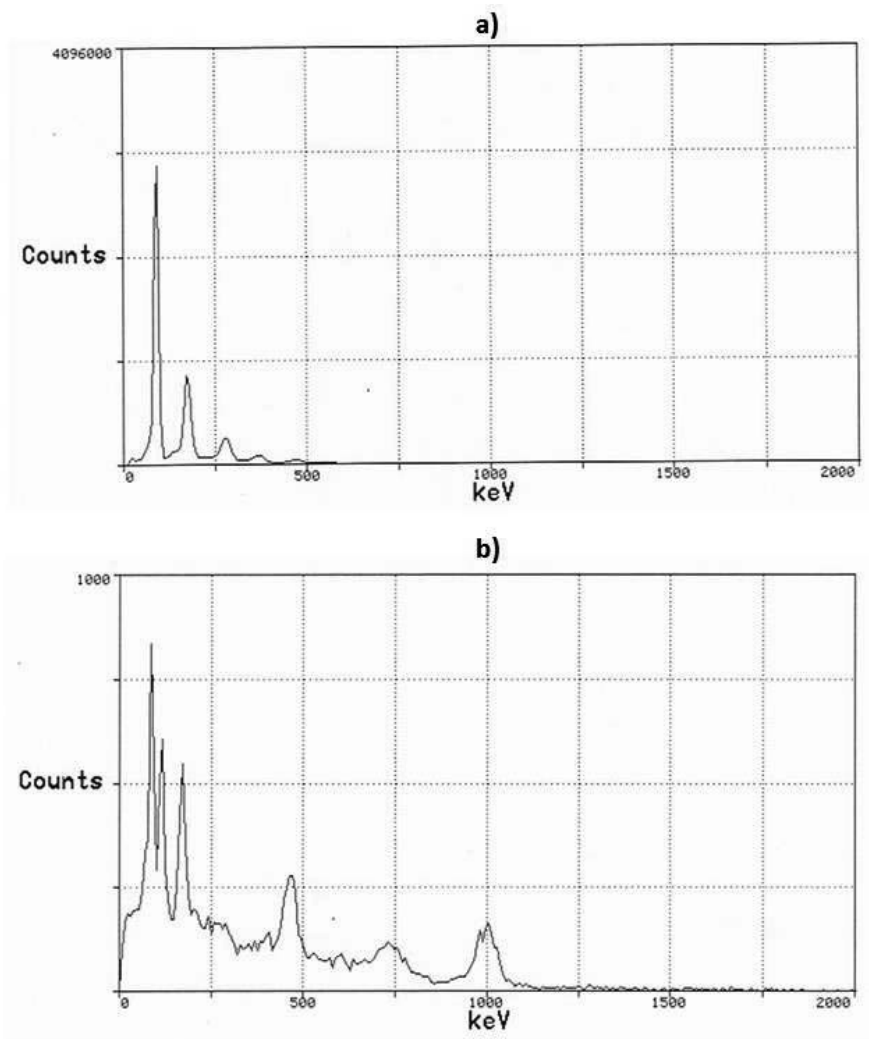
Figure 3.17 Well counter spectra of the Dowex resin used to retain gallium (a) and its waste solution, 1 ml sample (b).

The characteristic ^{67}Ga γ-ray energies of 93, 185, 300 and 393 keV are easily identified in the spectrum (a), where the registered net counts was 14728901 cpm (counts per minute). When comparing it to the waste specter (b), the presence of the same energy level gammas is uncertain, given the low net counts (18689 cpm). Even if considering that only 1 ml of the total 45 ml waste solution was analyzed, the conclusion would be the same. If assuming a rough estimation of 45 times more count events detected in the complete waste solution, its total net counts would only represent 5.7 % of the net counts registered with the Dowex resin.

If no significant levels of ^{67}Ga were identified in the waste, it is possible to corroborate the assumption that no significant levels of other gallium isotopes, such as ^{68}Ga, were lost in the resin absorption process.

4. Conclusion

Since the past years, the use of ^{68}Ga in PET radiopharmaceuticals has been showing very positive results for the image detection of neuroendocrine tumours. Seeking easier and less expensive methods for a high yield production of ^{68}Ga is continuously desirable.

The present work had the goal to study the feasibility of a cyclotron production of ^{68}Ga using a Zn-based liquid target. The target solution chosen was based on natural zinc chloride salt.

A material study of niobium was performed in order to evaluate its resistance conditions to zinc chloride solutions. The material is widely used in target chambers and windows for different target productions due to its optimal physicochemical properties. The results showed the corrosion effect of zinc chloride solutions, with the consequent formation of oxide structures in the material surface. Nevertheless, the extreme conditions of the exposure tests did not led to a destructive corrosion process on the samples surface, as proved by the mass, SEM and EDS analyses. Besides, the target chamber should only be exposed to the zinc chloride target solution for one hour per day, being thoroughly cleaned between irradiations. Thus, niobium was considered suitable to sufficiently resist the extreme conditions of the desired cyclotron target.

A degradation analysis of teflon, used to transport the irradiated solutions into hot-cells, was conducted as well. Two teflon samples were dipped in zinc chloride solutions and another in water for one month. The thermogravimetric analysis showed similar temperature-degradation behaviors for both control and test samples. Consequently, this proved the safety and resistance of the material for the transfer of the zinc chloride solutions.

In order to ensure the purification of the gallium isotopes produced within the irradiated target, different retention columns were studied. Initially, the columns were tested with dilutions of 0.025 M HCl (from the ^{68}Ge-^{68}Ga generator elution) and 5 M ZnCl$_2$ solutions with water. The results showed high gallium absorption levels for the Dowex 50W-X8 and Strata-XC ion exchange resins.

Initial irradiation test productions were conducted, ensuring the stability of the target inside the cyclotron, target transportation procedure and isotope production yields, specifically focusing on ^{68}Ga. Its half-life pattern and correspondent production yields were obtained by a non-linear regression method. The experiment achieved a result of 461.76 $\pm$ 46.62 MBq (12.48 $\pm$ 1.26 mCi) yield with a $t_{1/2\,exp}$ = 67.82 $\pm$ 0.50 min. The target irradiation was conducted with a proton beam integrated current of 6 μA h and a 1.6 ml target with a solute/solvent ratio of 1 g of zinc chloride to 1 ml of H$_2$O.

Ultimately, a final test procedure was done in order to evaluate the absorption of the Dowex 50W-X8 ion exchange resin for gallium elements, this time for the irradiated target solution. After the retention process, the resin analysis of the time-activity curves revealed the gallium half-life periods of 9.5 $\pm$ 0.2 hours and 67.4 $\pm$ 2.9 mins. Furthermore, the obtained production yields corresponded to 0.97 $\pm$ 0.10 mCi for ^{66}Ga and 2.59 $\pm$ 0.28 mCi for ^{68}Ga. No gallium isotopes were identified in the waste. These findings were supported from the spectroscopy analysis, four days after the final irradiation. ^{67}Ga characteristic γ-ray energies were highly detected in the resin, with no significant levels of the isotope present in the waste solution.

The conducted tests and analysis proved the feasibility of ^{68}Ga production in cyclotron, using a zinc chloride target based solution, further ensuring high absorption levels of gallium by a purification step using an ion exchange resin.

5. Future Perspectives

Although the production of ^{68}Ga with a zinc chloride liquid base target through a proton irradiation was proved to be possible, there are still many aspects to study and follow-up.

Additional studies should be performed in niobium to further evaluate the corrosion process based on the effect of zinc chloride. It is important to understand this effect with irradiation conditions (high pressure, temperature, agitation, etc.) on the niobium target window used. A comparison to the analysis results presented in this work should be performed.

Improving and optimizing the methods for ^{68}Ga production is necessary for the present approach to compete and surpass the traditional ^{68}Ge-^{68}Ga generator method. For that purpose, higher concentrations of zinc chloride target solutions should be prepared, taking advantage of the high solubility of $ZnCl_2$ in water. Although the proton energies used allow positive production yields, the beam conditions can still be improved. A study on the reaction cross sections should be conducted to further evaluate the proton beam energy range to achieve optimal ^{68}Ga production yields. But more importantly, ^{68}Ga production should be done with a highly pure and enriched $^{68}ZnCl_2$ solution target instead. In addition to increasing the irradiation yields, fewer impurities are formed, facilitating the later ^{68}Ga purification and radiolabeling processes, as expected. Besides, the basis of this work is to assess the possibility of producing and extract ^{68}Ga for an optimal $^{68}Zn(p,n)^{68}Ga$ reaction, initially evaluated with ^{nat}Zn.

One of the necessary goals to achieve in order to progress into a Zinc-68 enriched salt solution is to separate and reuse the post-production zinc elements waste for other irradiations. Otherwise, the elevated costs of the enriched solution would not be compensated. To that end, zinc purification methods need to be investigated and fully tested during several irradiations trials, using the same recovered zinc solution.

Despite the good results for the gallium absorption by using the Dowex 50W-X8 ion exchange resin, different methods should also be studied and tested. The Dowex elution with a 3.5 M HCl solution may not be suitable for the radiolabeling with DOTA peptides. Adding a second purification step, or assessing other useful approaches to retain and extract the produced ^{68}Ga, such as testing the Strata-XC resin, can be more helpful.

It is also impetuous to label the produced ^{68}Ga with DOTA peptides, since it is the main goal of this cyclotron production. The procedure should be similar to the one used with the ^{68}Ge-^{68}Ga generator. However, the quality control exams, such as high-performance liquid chromatography (HPLC), will be important to clarify the purity and label capacity of the final ^{68}Ga product into radiopharmaceutical peptides.

References

1. Klöppel, G., *Classification and pathology of gastroenteropancreatic neuroendocrine neoplasms.* Endocr Relat Cancer, 2011. **18 Suppl 1**: p. S1-16.

2. Klöppel, G., A. Perren, and P.U. Heitz, *The Gastroenteropancreatic Neuroendocrine Cell System and Its Tumors: The WHO Classification.* Annals of the New York Academy of Sciences, 2004. **1014**(1): p. 13-27.

3. Fraenkel, M., M.K. Kim, A. Faggiano, and G.D. Valk, *Epidemiology of gastroenteropancreatic neuroendocrine tumours.* Best Pract Res Clin Gastroenterol, 2012. **26**(6): p. 691-703.

4. Kim, J., et al., *Clinical features of 20 patients with curatively resected biliary neuroendocrine tumours.* Dig Liver Dis, 2011. **43**(12): p. 965-70.

5. Niederle, M.B. and B. Niederle, *Diagnosis and treatment of gastroenteropancreatic neuroendocrine tumors: current data on a prospectively collected, retrospectively analyzed clinical multicenter investigation.* Oncologist, 2011. **16**(5): p. 602-13.

6. Tonnhofer, U., C. Balassy, C.A. Reck, A. Koller, and E. Horcher, *Neuroendocrine tumor of the common hepatic duct, mimicking a choledochal cyst in a 6-year-old child.* J Pediatr Surg, 2009. **44**(6): p. E23-5.

7. Fernández-Cruz, L., J. Romero, R. Zelaya, C. Olvera, and L. Maglio, *Surgical strategies for nonfunctioning neuroendocrine pancreatic tumors and for other pancreatic neoplasms associated with multiple endocrine neoplasia type 1.* The American Journal of Surgery, 2007. **194**(4): p. S143-S147.

8. Gabriel, M., et al., *68Ga-DOTA-Tyr3-Octreotide PET in Neuroendocrine Tumors: Comparison with Somatostatin Receptor Scintigraphy and CT.* Journal of Nuclear Medicine, 2007. **48**(4): p. 508-518.

9. Modlin, I.M., M. Pavel, M. Kidd, and B.I. Gustafsson, *Review article: somatostatin analogues in the treatment of gastroenteropancreatic neuroendocrine (carcinoid) tumours.* Aliment Pharmacol Ther, 2010. **31**(2): p. 169-88.

10. Modlin, I.M., et al., *Gastroenteropancreatic neuroendocrine tumours.* The Lancet Oncology, 2008. **9**(1): p. 61-72.

11. Rockall, A.G. and R.H. Reznek, *Imaging of neuroendocrine tumours (CT/MR/US).* Best Pract Res Clin Endocrinol Metab, 2007. **21**(1): p. 43-68.

12. Seeram, E., *Computed Tomography: Physical Principles and Recent Technical Advances.* Journal of Medical Imaging and Radiation Sciences, 2010. **41**(2): p. 87-109.

13.   Akata, S., et al., *Computed tomographic findings of large cell neuroendocrine carcinoma of the lung.* Clin Imaging, 2007. **31**(6): p. 379-84.

14.   MacDonald-Jankowski, D.S., *Magnetic Resonance Imaging. Part 1: the Basic Principles.* Asian Journal of Oral and Maxillofacial Surgery, 2006. **18**(3): p. 165-171.

15.   Metz, D.C. and R.T. Jensen, *Gastrointestinal neuroendocrine tumors: pancreatic endocrine tumors.* Gastroenterology, 2008. **135**(5): p. 1469-92.

16.   Sundin, A., *Radiological and nuclear medicine imaging of gastroenteropancreatic neuroendocrine tumours.* Best Pract Res Clin Gastroenterol, 2012. **26**(6): p. 803-18.

17.   Pantaleo, M.A., et al., *Conventional and novel PET tracers for imaging in oncology in the era of molecular therapy.* Cancer Treat Rev, 2008. **34**(2): p. 103-21.

18.   van Loon, J., et al., *Therapeutic implications of molecular imaging with PET in the combined modality treatment of lung cancer.* Cancer Treat Rev, 2011. **37**(5): p. 331-43.

19.   Phelps, M.E., *Positron emission tomography provides molecular imaging of biological processes.pdf.* Inaugural Articles of the National Academy of Sciences, 2000.

20.   Valk, P.E., D.L. Baily, D.W. Townsend, and M.N. Maisey, *Positron Emission Tomography: Basic Sciences*. 2003: Springer.

21.   Zanzonico, P., *Positron emission tomography: a review of basic principles, scanner design and performance, and current systems.* Seminars in Nuclear Medicine, 2004. **34**(2): p. 87-111.

22.   Li, Z. and P.S. Conti, *Radiopharmaceutical chemistry for positron emission tomography.* Adv Drug Deliv Rev, 2010. **62**(11): p. 1031-51.

23.   E. Phelps, M., *Positron emission tomography provides molecular imaging of biological processes.* Inaugural Articles of the National Academy of Sciences, 2000.

24.   Wadsak, W. and M. Mitterhauser, *Basics and principles of radiopharmaceuticals for PET/CT.* Eur J Radiol, 2010. **73**(3): p. 461-9.

25.   Tewson, T.J. and K.A. Krohn, *PET radiopharmaceuticals state-of-the-art and future prospects.* Seminars in Nuclear Medicine, 1998. **28**(3): p. 221-234.

26.   Unak, T., *Recent advances in medical radionuclide production and future perspective of compact medical cyclotrons.* Progres in Nuclear Energy, 1970. **37**(1): p. 333-337.

27.   Khan, M.U., et al., *Clinical indications for Gallium-68 positron emission tomography imaging.* Eur J Surg Oncol, 2009. **35**(6): p. 561-7.

28.   Sanchez-Crespo, A., *Comparison of Gallium-68 and Fluorine-18 imaging characteristics in positron emission tomography.* Appl Radiat Isot, 2013. **76**: p. 55-62.

29.   de Blois, E., et al., *Characteristics of SnO2-based 68Ge/68Ga generator and aspects of radiolabelling DOTA-peptides.* Appl Radiat Isot, 2011. **69**(2): p. 308-15.

30. Prata, M.I., *Gallium-68: A New Trend in PET Radiopharmacy.* Current Radiopharmaceuticals, 2012. **5**(3).

31. Sadeghi, M., T. Kakavand, S. Rajabifar, L. Mokhtari, and A. Rahimi-Nezhad, *Cyclotron production of 68Ga via proton-induced reaction on 68Zn target.* NUKLEONIKA, 2009. **54**(1): p. 25-28.

32. Breeman, W.A., et al., *(68)Ga-labeled DOTA-peptides and (68)Ga-labeled radiopharmaceuticals for positron emission tomography: current status of research, clinical applications, and future perspectives.* Semin Nucl Med, 2011. **41**(4): p. 314-21.

33. Al-Nahhas, A., et al., *What can gallium-68 PET add to receptor and molecular imaging?* Eur J Nucl Med Mol Imaging, 2007. **34**(12): p. 1897-901.

34. Schreiter, N.F., et al., *Cost comparison of 111In-DTPA-octreotide scintigraphy and 68Ga-DOTATOC PET/CT for staging enteropancreatic neuroendocrine tumours.* Eur J Nucl Med Mol Imaging, 2012. **39**(1): p. 72-82.

35. Modlin, I.M., M. Kidd, I. Latich, M.N. Zikusoka, and M.D. Shapiro, *Current Status of Gastrointestinal Carcinoids.* Gastroenterology, 2005. **128**(6): p. 1717-1751.

36. Warner, R.R.P., *Enteroendocrine Tumors Other Than Carcinoid: A Review of Clinically Significant Advances.* Gastroenterology, 2005. **128**(6): p. 1668-1684.

37. Rufini, V., M.L. Calcagni, and R.P. Baum, *Imaging of neuroendocrine tumors.* Semin Nucl Med, 2006. **36**(3): p. 228-47.

38. Al-Nahhas, A., et al., *Gallium-68 PET: A New Frontier in Receptor Cancer Imaging.* ANTICANCER RESEARCH, 2007. **27**: p. 4087-4094.

39. Wild, D., et al., *Comparison of 68Ga-DOTANOC and 68Ga-DOTATATE PET/CT within patients with gastroenteropancreatic neuroendocrine tumors.* J Nucl Med, 2013. **54**(3): p. 364-72.

40. de Araujo, E.B., et al., *A comparative study of 131I and 177Lu labeled somatostatin analogues for therapy of neuroendocrine tumours.* Appl Radiat Isot, 2009. **67**(2): p. 227-33.

41. Grozinsky-Glasberg, S., A.B. Grossman, and M. Korbonits, *The role of somatostatin analogues in the treatment of neuroendocrine tumours.* Mol Cell Endocrinol, 2008. **286**(1-2): p. 238-50.

42. Theodoropoulou, M. and G.K. Stalla, *Somatostatin receptors: From signaling to clinical practice.* Front Neuroendocrinol, 2013. **34**(3): p. 228-52.

43. Capello, A., E.P. Krenning, W.A. Breeman, B.F. Bernard, and M. de Jong, *Peptide Receptor Radionuclide Therapy In Vitro Using [111In-DTPA0]Octreotide.* J Nucl Med, 2003. **44**: p. 98-104.

44. Fanti, S., et al., *Evaluation of unusual neuroendocrine tumours by means of 68Ga-DOTA-NOC PET.* Biomed Pharmacother, 2008. **62**(10): p. 667-71.

45.   Banerjee, S.R. and M.G. Pomper, *Clinical applications of Gallium-68.* Appl Radiat Isot, 2013. **76**: p. 2-13.

46.   Decristoforo, C., R.D. Pickett, and A. Verbruggen, *Feasibility and availability of (6)(8)Ga-labelled peptides.* Eur J Nucl Med Mol Imaging, 2012. **39 Suppl 1**: p. S31-40.

47.   Veksler, V.A., *Principles of acceleration of charged particles.* The Soviet Journal of Atomic Energy, 1996. **1**(1): p. 77-83.

48.   Ibrahim, M.M., *Control and characterization of a Cyclotron proton beam*, 2010, University of Missouri-Columbia.

49.   King, B.T., *A Preliminary design for a small permanent magnet Cyclotron*, in *Department of Physics*2003, Houghton College.

50.   Strickmans, K., *The isochronous cyclotron: principles and recent developments.* Computerized Medical Imaging and Graphics, 2000. **25**: p. 69-78.

51.   Halgamunge, M.N., *Effect of Cyclotron Resonance Frequencies in Particles Due to AC and DC Electromagnetic Fields.* International Journal of Electrical and Computer Engineering, 2010. **5**(3).

52.   Doster, J.M., *Deployment, Testing and Analysis of Advanced Thermosyphon Target Systems for Production of Aqueous [18F]Fluoride via 18O(p,n)18F*, 2008: North Carolina State University.

53.   Cloquet, C., J. Carignan, M.F. Lehmann, and F. Vanhaecke, *Variation in the isotopic composition of zinc in the natural environment and the use of zinc isotopes in biogeosciences: a review.* Anal Bioanal Chem, 2008. **390**(2): p. 451-63.

54.   Lide, D.R., ed., *CRC Handbook of Chemistry and Physics*. 2005.

55.   Jakubke , H.-D., ed, *Concise Encyclopedia Chemistry*. 1994.

56.   Holeman, A.F., *Inorganic chemistry*, ed. E. Wiberg and N. Wiberg. 2001, San Diego: Academic Press.

57.   Graham, R.A. and R.C. Sutherlin, *Niobium and Niobium alloys in corrosive applications*, Wah Chang, An Allegheny Technologies Company.

58.   Zeisler, S.K., D.W. Becker, R.A. Pavan, R. Moschel, and H. Rühle, *A water-cooled spherical niobium target for the production of [18F]fluoride.* Applied Radiation and Isotopes, 2000. **53**(3): p. 449-453.

59.   Kim, D.H., S.J. Kim, and S.K. Oh, *Image improvement with modified scanning waves and noise reduction in a scanning electron microscope.* Nuclear Instruments and Methods in Physics Research, 2010. **620**: p. 112-120.

60.   Bogner, A., P.H. Jouneau, G. Thollet, D. Basset, and C. Gauthier, *A history of scanning electron microscopy developments: towards "wet-STEM" imaging.* Micron, 2007. **38**(4): p. 390-401.

61. Hollerith, C., et al., *Energy dispersive X-ray spectroscopy with microcalorimeters.* Nuclear Instruments and Methods in Physics Research Section A: Accelerators, Spectrometers, Detectors and Associated Equipment, 2004. **520**(1-3): p. 606-609.

62. Saito, F., et al., *Electrochemical transfer of (18)F from (18)O water to aprotic polar solvent.* Appl Radiat Isot, 2007. **65**(5): p. 524-7.

63. Brown, E.N. and D.M. Dattelbaum, *The role of crystalline phase on fracture and microstructure evolution of polytetrafluoroethylene (PTFE).* Polymer, 2005. **46**(9): p. 3056-3068.

64. Stawski, D., *The effect of sample weight in thermogravimetric analysis of low viscosity polypropylene in air atmosphere.* Polymer Testing, 2009. **28**(2): p. 223-225.

65. Anandhan, S., *Thermal Analysis*, 2012, Dept. of Met. and Mat. Engg., NITK.

66. Damartzis, T., D. Vamvuka, S. Sfakiotakis, and A. Zabaniotou, *Thermal degradation studies and kinetic modeling of cardoon (Cynara cardunculus) pyrolysis using thermogravimetric analysis (TGA).* Bioresour Technol, 2011. **102**(10): p. 6230-8.

67. Alchin, D., *Ion exchange resins.* New Zeland Institue of Chemistry, 2008.

68. Persson, M., J. Madsen, S. Ostergaard, M. Ploug, and A. Kjaer, *68Ga-labeling and in vivo evaluation of a uPAR binding DOTA- and NODAGA-conjugated peptide for PET imaging of invasive cancers.* Nucl Med Biol, 2012. **39**(4): p. 560-9.

69. Das, M.K., S. Chattopadhayay, B.R. Sarkar, and N. Ramamoorthy, *A Cation Exchange Method for Separation of llln from Inactive Silver, Copper, Traces of Iron and Radioactive Gallium and Zinc Isotopes.* Applied Radiation and Isotopes, 1996. **48**(1): p. 11-14.

70. Massoud, A., F. Abou El-Nour, H. Killa, and U. Seddik, *Chromatographic separation of In(III) from Cd(II) in aqueous solutions using commercial resin (Dowex 50W-X8).* Central European Journal of Chemistry, 2010. **8**(3): p. 696-701.

71. Chattopadhayay, S., M.K. Das, B.R. Sarkar, and N. Ramamoorthy, *Simple procedure for the preparation of iron-free 67Ga from an irradiated copper target—Use of ascorbic acid.* Appl. Radiat. Isot., 1997. **48**(2): p. 211-212.

72. Levkovskij, V.N., *Activation cross section nuclides of average masses (A=40-100)by protons and alpha-particles with average energies (E=10-50 MeV).* 1991, Moscow: Levkovskij.

73. Al-Saleh, F.S., K.S. Al Mugren, and A. Azzam, *Excitation function measurements and integral yields estimation for natZnp,x reactions at low energies.* Appl Radiat Isot, 2007. **65**(10): p. 1101-7.

74. Simpson, B.R.S. and T.P. Ntsoane, *Decay scheme of 67Ga.* Applied Radiation and Isotopes, 2000. **52**(2000): p. 551-556.

75. Yalcin, P. and Y. Kurucu, *Emission probabilities of K X- and gamma-rays following 51Cr and 67Ga decay.* Appl Radiat Isot, 2005. **62**(1): p. 63-7.

76.   Bieber, R., C. Wagemans, and G. Goemine, *Thermal neutron induced (n,p) and (n,a) reactions on 37Ar.* Nuclear Physics A, 1999. **647**: p. 3-11.

77.   Matsumoto, J., *Electrochemistry of intermetallic phases of Ni-Cr-Fe alloys in aqueous environment*, in *Department of Nuclear Engineering*1982, Waseda University: Tokyo, Japan.

78.   Vasiliovych, C., *Attempts for the electrodeposition of niobium from ionic liquids*, 2010, Università Degli Studi di Padova: Istituto Nazionale di Fisica Nucleare.

79.   Palacios, C., K. Wigertz, B. Martin, and C.M. Weaver, *Sweat mineral loss from whole body, patch and arm bag in white and black girls.* Nutrition Research, 2003. **23**(3): p. 401-411.

80.   Jeske, H., A. Schirp, and F. Cornelius, *Development of a thermogravimetric analysis (TGA) method for quantitative analysis of wood flour and polypropylene in wood plastic composites (WPC).* Thermochimica Acta, 2012. **543**: p. 165-171.

81.   Chipara, M., K. Lozano, A. Hernandez, and M. Chipara, *TGA analysis of polypropylene– carbon nanofibers composites.* Polymer Degradation and Stability, 2008. **93**(4): p. 871-876.

82.   Engle, J.W., et al., *Very high specific activity (6)(6)/(6)(8)Ga from zinc targets for PET.* Appl Radiat Isot, 2012. **70**(8): p. 1792-6.

83.   Martins, P., *Desenvolvimento de método para separação química de Gálio-67 pela técnica de difusão térmica*, in *Instituto de Pesquisas Energéticas e Nucleares*2012, Universidade de São Paulo.